Crossed Corticostriatal Projections in the Macaque Brain

The Journal of Neuroscience

https://jneurosci.msubmit.net

JN-RM-0071-22R2

Crossed corticostriatal projections in the macaque brain

Elena Borra, Universita degli Studi di Parma Dipartimento di Medicina e Chirurgia
Dalila Biancheri, Università degli studi di Parma
Marianna Rizzo, Universita degli Studi di Parma
Fabio Leonardi, Università degli Studi di Parma
Giuseppe Luppino, Universita degli Studi di Parma

Commercial Interest:

Crossed corticostriatal projections in the macaque brain.

Elena Borra[1], Dalila Biancheri[1], Marianna Rizzo[1], Fabio Leonardi[2] and Giuseppe Luppino[1]

[1]Dipartimento di Medicina e Chirurgia, Unità di Neuroscienze, Università di Parma, 43100 Parma, Italy; [2]Dipartimento di Scienze Medico-Veterinarie, Università di Parma, 43100 Parma, Italy.

Corresponding author: Prof. Elena Borra. E mail: elena.borra@unipr.it

Abbreviated title: Crossed CSt projections in the macaque

Keywords: Monkey; Basal Ganglia; Striatum; Interhemispheric transfer; Frontal cortex; Cingulate cortex

Number of figures and tables: 12 Figures, 3 Tables

Number of pages: 33

Number of words: in abstract (199), introduction (536), discussion (1557)

Conflict of interest: The authors declare no competing financial interests.

Acknowledgements

This work was supported by University of Parma and cosponsored by Fondazione Cariparma (Programme "FIL 2019 - Quota Incentivante") to GL and by Ministero dell'Istruzione, dell'Università e della Ricerca (Grant number: PRIN 2017, n°2017KZNZLN_002) to EB. The 3D reconstruction software was developed by CRS4, Pula, Cagliari, Italy. The authors thank Giuseppe Pedrazzi for advices on statistical analysis.

ABSTRACT

In non-human primates, major input to the striatum originates from ipsilateral cortex and thalamus. The striatum is a target also of "crossed" corticostriatal (CSt) projections from the contralateral hemisphere, which have been so far somewhat neglected. In the present study, based on neural tracer injections in different parts of the striatum in macaques of either sex, we analyzed and compared qualitatively and quantitatively the distribution of labeled CSt cells in the two hemispheres. The results showed that crossed CSt projections to the caudate and the putamen can be relatively robust (up to 30% of total labeled cells). The origin of the direct and the crossed CSt projections was not symmetrical as the crossed ones originated almost exclusively from motor, prefrontal, and cingulate areas and not from parietal and temporal areas. Furthermore, there were several cases in which the contribution of contralateral areas tended to equal that of the ipsilateral ones. The present study is the first detailed description of this anatomical pathway of the macaque brain and provides the substrate for bilateral distribution of motor, motivational, and cognitive signals for reinforcement learning and selection of actions or action sequences, and for learning of compensatory motor strategies after cortical stroke.

SIGNIFICANT STATEMENT

In non-human primates the striatum is a target of projections originating from the contralateral hemisphere (*crossed* CSt projections), which have been so far poorly investigated. The present study analyzed qualitatively and quantitatively in the macaque brain the origin of the crossed CSt projections compared to those originating from the ipsilateral hemisphere. The results showed that crossed CSt projections originate mostly from frontal and rostral cingulate areas and in some cases their contribution tended to equal that from ipsilateral areas. These projections could provide the substrate for bilateral distribution of motor, motivational, and cognitive signals for reinforcement learning and action selection, and for learning of compensatory motor strategies after cortical stroke.

INTRODUCTION

The identification of all the inputs to the striatum and the way in which they distribute in the various parts of it, is an essential aspect for understanding the mode of information processing in the basal ganglia for different motor and non-motor functions.

The ipsilateral cerebral cortex is certainly the major source of afferents to the striatum. Early studies of these corticostriatal (CSt) projections in non-human primates have favored a "parallel processing" model in which different striatal territories are a target of specific cortical regions and, in turn, are at the origin of largely segregated basal ganglia-thalamo-cortical loops (Alexander et al., 1986).

Subsequent studies have suggested a "parallel processing and information convergence" model (see Nambu 2011) in which each main basal ganglia-thalamo-cortical loop consists of several largely segregated closed subloops. Each subloop originates from, and projects to limited sets of closely related areas and involves distinct, relatively restricted striatal zones, which have been referred to as "input channels" (Strick et al. 1995; Middleton and Strick 2000).

More recent studies showed an even more complex pattern of information convergence in the primate striatum. First, there is evidence for overlap in restricted striatal zones of projection fields of distant, interconnected areas jointly involved in specific large-scale functionally specialized cortical networks (Gerbella et al., 2016; Choi et al., 2017). Second, the laminar origin of the CSt projections from a given area can largely vary according to the target striatal zone so that different striatal zones are targets of characteristically weighted laminar projections from the various input areas (Borra et al., 2021).

The striatum is also a target of "crossed" CSt projections originating from the contralateral hemisphere. Though noted in the macaque brain since at least fifty years (e.g., Kemp and Powell 1970), these projections have been so far somewhat neglected. Indeed, crossed CSt projections in the macaque brain have been reported in several studies after anterograde tracer injections in different cortical areas (e.g., Künzle, 1975; 1978; Liles and Updyke, 1985; Huerta and Kaas, 1990;

Cavada and Goldman-Rakic, 1991; McGuire et al., 1991; Parthasarathy et al. 1992). However, these studies could not give a comprehensive qualitative and quantitative view of the regional origin of these projections to the various parts of the striatum. To our knowledge, Jones et al. (1977) have been the only ones in describing the origin of the crossed CSt projections based on retrograde tracer injections in the putamen in squirrel monkeys. However, this description was only qualitative and shown for only one subject.

Accordingly, it is still largely unknown which is the effective size of the crossed CSt projections compared to the "direct" ones, whether crossed CSt projections originate from all the cortical areas that project to the ipsilateral striatum, and whether the origin of crossed and direct CSt projections to a given striatal zone is symmetrical. Thus, it is still an open question whether crossed CSt projections could represent a potentially important variable to consider in defining the pattern of information convergence in the striatum.

To address these issues, in the present study we have placed retrograde tracer injections in different parts of the striatum and compared qualitatively and quantitatively the regional distribution of the labeled CSt cells in the contralateral vs. the ipsilateral hemisphere.

METHODS

Subjects, surgical procedures, and selection of the injection sites

The experiments were carried out in four *Macaca mulatta* (Cases 71 female, 75, 76, and 77 male), in which retrograde neural tracers were injected in different parts of the caudate and putamen. Animal handling as well as surgical and experimental procedures complied with the European law on the humane care and use of laboratory animals (directives 86/609/EEC, 2003/65/CE, and 2010/63/EU) and Italian laws in force regarding the care and use of laboratory animals (D.L. 116/92 and 26/2014), were periodically approved by the Veterinarian Animal Care and Use Committee of the University of Parma and authorized by the Italian Ministry of Health.

Before the injection of neural tracers, we obtained scans of each brain using magnetic resonance imaging (MRI; 7 T General Electric, Boston, MA) to calculate the stereotaxic coordinates of the striatal target regions and the best trajectory of the needle to reach it.

Under general anesthesia (Case 71: Zoletil®, initial dose 20 mg/kg, i.m., supplemental 5–7 mg/kg/hr, i.m.; Cases 75, 76 and 77: induction with Ketamine 10 mg/kg, i.m. followed by intubation, isoflurane 1.5–2%) and aseptic conditions, each animal was placed in a stereotaxic apparatus and an incision was made in the scalp. The skull was trephined to remove the bone and the dura was opened to expose a small cortical region. After tracer injections, the dural flap was sutured, the bone was replaced, and the superficial tissues were sutured in layers. During surgery, hydration was maintained with saline, and heart rate, blood pressure, respiratory depth, and body temperature were continuously monitored. Upon recovery from anesthesia, the animals were returned to their home cages and closely observed. Dexamethasone (0.5 mg/kg, i.m.) and prophylactic broad-spectrum antibiotics (e.g., Ceftriaxone 80 mg/kg, i.m.) were administered pre- and postoperatively, as were analgesics (e.g., Ketoprofen 5 mg/kg i.m.).

Tracer injections and histological procedures

Based on stereotaxic coordinates, the neural tracers Fast Blue (FB, 3% in distilled water, Dr Illing Plastics GmbH, Breuberg, Germany), Diamidino Yellow (DY, 2% in 0.2M phosphate buffer

121 at pH 7.2, Dr Illing Plastics), Wheat Germ Agglutinin (WGA; 4% in distilled water, Vector
122 Laboratories, Burlingame, CA), Dextran conjugated with Lucifer Yellow (Lucifer Yellow Dextran,
123 LYD, 10 000 MW, 10% 0.1M phosphate buffer, pH 7.4; Invitrogen, Thermo Fisher Scientific,
124 Waltham, MA), and Cholera Toxin B subunit, conjugated with Alexa 488 (CTB green, CTBg; 1%
125 in 0.01 M phosphate-buffered saline at pH 7.4, Molecular Probes, Thermo Fisher Scientific) were
126 slowly pressure-injected through a stainless steel 31 gauge beveled needle attached through a
127 polyethylene tube to a Hamilton syringe (Hamilton Company, Reno NV). For all tracer injections,
128 the needle was lowered to the striatum within a guiding tube, to avoid tracer spill-over in the white
129 matter. Table 1 summarizes the locations of the injections, the injected tracers, and the amounts
130 injected.
131 After appropriate survival periods following the injections (48 hours for WGA, 21-28 days for
132 the other tracers, see Table 1), each animal was deeply anesthetized with an overdose of sodium
133 thiopental and perfused through the left cardiac ventricle consecutively with saline (about 2 L in 10
134 min), 3.5% formaldehyde (5 L in 30 min), and 5% glycerol (3 L in 20 min), all prepared in 0.1 M
135 phosphate buffer, pH 7.4. Each brain was then blocked coronally on a stereotaxic apparatus,
136 removed from the skull, photographed, and placed in 10% buffered glycerol for 3 days and 20%
137 buffered glycerol for 4 days. In Case 75, the right inferotemporal cortex was removed for other
138 experimental purposes. Finally, each brain was cut frozen into coronal sections of 60-µm (Case 75)
139 or 50-µm (Cases 71, 76 and 77) thickness.
140 In all cases, sections spaced 300 µm apart - that is one section in each repeating series of 6 in
141 Cases 71, 76, and 77 and one in series of 5 in Case 75 - were mounted, air-dried, and quickly
142 coverslipped for fluorescence microscopy. Other series of sections spaced 300 µm apart were
143 processed for visualizing CTBg (Cases 75, 76 and 77), LYD (Case 75), or WGA (Cases 76 and 77)
144 with immunohistochemistry. Specifically, in all sections endogenous peroxidase activity was
145 eliminated by incubation in a solution of 0.6% hydrogen peroxide and 80% methanol for 15 min at
146 room temperature. For the visualization of CTBg, the sections were then incubated for 72 h at 4°C

147 in a primary antibody solution of rabbit anti-Alexa 488 (1:15000, Thermo Fisher Scientific) in 0.5%
148 Triton, 5% normal goat serum in PBS, and for 1 h in biotinylated secondary antibody (1:200,
149 Vector) in 0.3% Triton, 5% normal goat serum in PBS. For the visualization of LYD, the sections
150 were then incubated for 96 h at 4°C in a primary antibody solution of or rabbit anti-LY (1:3000;
151 Life Technologies, Thermo Fisher Scientific) in 0.5%Triton, 5% normal goat serum in phosphate
152 buffer (PB) 0,1M, and for 1 h in biotinylated secondary antibody (1:200, Vector) in 0.3% Triton,
153 5% normal goat serum in PB. For the visualization of the WGA, the sections were incubated
154 overnight at room temperature in a primary antibody solution of goat anti-WGA (1:2000, Vector) in
155 0.3% Triton, 5% normal rabbit serum in PBS and for 1 h in biotinylated secondary antibody (1:200,
156 Vector) in 0.3% Triton, 5% normal rabbit serum in PBS. Finally, in all sections the labeling was
157 visualized using the Vectastain ABC kit (Vector) and then a solution of DAB (50mg/100 ml; Sigma
158 Millipore), 0.01% hydrogen peroxide, 0.02% cobalt chloride, and 0.03% nickel ammonium sulfate
159 in 0.1 M PB.

160 In all cases, one series of each sixth section (fifth section in Case 75) was stained with the Nissl
161 method (0.1% thionin in 0.1 M acetate buffer, pH 3.7).

162 **Data analysis**

163 *Injection sites, distribution of retrogradely labeled neurons, and areal attribution of the labeling*

164 All the injection sites used in this study shown in Figure 1 were completely restricted to the
165 target striatal nucleus (caudate or putamen). The cortical distribution of retrograde labeling in the
166 ipsilateral and contralateral hemisphere was plotted in sections every 600 μm (every 1200 μm in
167 Case 75l LYD) together with the outer and inner cortical borders, using a computer-based charting
168 system. Data from individual sections were then imported into the 3-dimensional (3D)
169 reconstruction software (Demelio et al. 2001) providing volumetric reconstructions of the monkey
170 brain, including connectional and architectonic data.

171 The criteria and maps adopted for the areal attribution of the labeling were similar to those
172 adopted in previous studies (see Borra et al., 2017; Caminiti et al., 2017). Specifically, prefrontal,

frontal and cingulate motor, and opercular frontal areas, where most of the labeling was located, were defined according to cyto- and/or chemo-architectonic criteria described in Matelli et al. (1985; 1991), Carmichael and Price (1994), Gerbella et al. (2007), Belmalih et al. (2009), and Saleem et al. (2014). Some prefrontal and cingulate areas have been considered together and referred to as 9/8B, 24/32, 24a/b, 24c/d, 23a/b, 23/31, and 29/30. In the inferior parietal lobule, the gyral convexity areas were defined according to cyto- and chemoarchitectonic criteria described in Gregoriou et al. (2006) and those of the lateral bank of the intraparietal sulcus based on connectional criteria described in Borra et al. (2008). The superior and medial parietal cortex were defined according to architectonic criteria described in Pandya and Seltzer (1982) and Luppino et al. (2005). For the caudal cingulate cortex, we adopted the cytoachitectonic map proposed by Morecraft et al. (2004). Finally, the temporal labeling in the STS cortex was attributed based on the electrophysiological and architectonic map proposed by Boussaoud et al. (1990) and guided by the atlas of Saleem and Logothetis (2012) and the labeling in the superior temporal gyrus (STG) and auditory belt cortex based on the architectonic, functional and connectional map described by Kaas and Hackett (2000; see also Saleem et al. 2008). For the quantitative analysis, the temporal lobe was subdivided into four regions: temporal pole (Tp), medial temporal (Tm), superior temporal (Ts), and inferior temporal (Ti).

Quantitative analysis and laminar distribution of the labeling

In all cases, the number of labeled neurons plotted in the ipsilateral and contralateral hemisphere was counted and the cortical input to the injected striatal zone was then expressed in terms of the percentage of labeled neurons found in each cortical subdivision, with respect to the overall cortical labeling found for each tracer injection in the ipsilateral hemisphere or in both ipsilateral and contralateral hemispheres.

For the areas where the percentage of ipsi + contra labeling was >1%, the number of labeled cells observed in the contralateral area was subdivided by the total number (ipsi + contra) of labeled

198 cells in order to obtain a “contralaterality index”, which could range from 1 (all cells in the
199 contralateral area) to 0 (all cells in the ipsilateral area).
200

RESULTS

Crossed CSt projections have been observed in all the cases of the present study. The proportion of labeled cells in the contra- vs. ipsilateral hemisphere largely varied according to the location of the injection site, showing a gradient in which crossed CSt projections were strongest to the caudate head and body, less strong to the rostral putamen and dorsal motor putamen and lowest to the middle or mid-ventral motor putamen, where the hand is represented (Alexander and De Long, 1985). In general, the distribution of the labeled CSt cells in the contralateral hemisphere differed for several aspects from that observed in the ipsilateral hemisphere (Figure 2). Indeed, contralateral areas with CSt projections were always a subset of the ipsilateral areas with CSt projections. Specifically, in all the cases, the areas in the posterior parietal, temporal, and insular cortex that exhibited even relatively robust labeling in the ipsilateral hemisphere had virtually no labeling in the contralateral hemisphere (Figure 2). Nevertheless, there were areas in the contralateral hemisphere whose relative contribution to the crossed CSt projections was much higher than that of the homolog ipsilateral areas to the direct CSt projections. The frequency distributions of the labeled CSt cells per area in the ipsilateral and the contralateral hemisphere were compared by the Pearson's chi-square test and likelihood ratio chi-square test (Figure 2). Both test showed a statistically significant difference ($p < 0.001$) among the distributions in all the cases.

CSt projections to the caudate nucleus

Two tracer injections were placed in the caudate head. In Case 76r the WGA injection site was slightly more rostral and medial than the LYD injection site of Case 75l (Fig. 1). As largely expected, in the ipsilateral hemisphere the highest proportion of labeled cells was located in the prefrontal cortex (Figs. 3 and 4 and Table 2), mostly involving areas 9/8B, followed by the rostral cingulate cortex, mostly involving the rostral area 24/32 and the rostral cingulate gyrus (area 24a/b). Relatively robust labeling was also observed in the temporal cortex involving in both cases belt/parabelt auditory areas, the superior temporal polysensory area (STP) and the medial temporal

cortex and, in Case 75l LYD, the rostral inferotemporal cortex. Much weaker was the labeling observed in rostral premotor, insular, and caudal cingulate cortex and, in Case 75l LYD, in the parietal cortex. In both cases, the percentage of labeled CSt cells observed in the contralateral hemisphere was robust, i.e., about 30% of the total number of ipsi- plus contralateral CSt cells (Figs. 3, 4 and Table 3).

In the contralateral hemisphere virtually all the labeling was located in frontal and cingulate areas whereas the parietal, temporal, and insular cortex were virtually devoid of labeling (Table 3). In both cases the labeling in the contralateral hemisphere was mostly concentrated in the rostral cingulate areas 24/32 and in prefrontal areas 9/8B, which were the most densely labeled areas in the ipsilateral hemisphere (Fig. 5). In both cases these two contralateral areas were among the five most labeled ones. However, in contralateral area 10 in Case 76r WGA and in areas 12o/12l in Case 75l LYD the labeling was relatively much weaker compared to the ipsilateral hemisphere. Weaker labeling also involved rostral premotor areas and the caudal cingulate cortex.

In Case 75r DY, the injection site was located in the caudate body at about the level of the AC (Fig. 1). The distribution of the labeling in the ipsilateral hemisphere (Fig. 6 and Table 2) was markedly different from that observed in the two cases previously described, involving mostly dorsal and medial premotor areas, primarily areas F3, F2, and F6 and to a lesser extent area F7. In area F3, the labeling mostly involved its rostral half. Less dense labeling was located in the ventral premotor cortex, motor cingulate (24c/d), inferior parietal (AIP, PFG, PG) and caudal superior parietal (PEc, PEci, PGm, V6A) areas. This labeling distribution suggests that the injection site involved a striatal sector related to visuo- and somatomotor control of arm movements. Also in this case, the labeling in the contralateral hemisphere was quite robust (about 30% of the ipsi- + contralateral CSt labeled cells) and was virtually all located in frontal and cingulate areas (Table 3). Specifically, the areal distribution of the labeled CSt cells (Fig. 5) in all the various premotor and cingulate areas was quite similar in the two hemispheres and contralateral areas F2 and F3 were among the five most labeled areas, considering both the ipsilateral and contralateral hemisphere.

CSt projections to the putamen

Five tracer injections involved the putamen, one more rostrally (Case 77r WGA) and the others at the same level of or caudal to the AC, at different dorso-ventral levels (Fig. 1).

The injection site in Case 77r WGA was located relatively ventrally in the pre-commissural putamen. In the ipsilateral hemisphere (Fig. 7), the labeling was densest in the premotor cortex, especially area F5, frontal operculum, and rostral cingulate cortex, especially area 24c/d. Less dense labeling involved prefrontal, parietal, and insular cortex and, more weakly, temporal and caudal cingulate cortex. The very weak labeling in area F1 suggests that the injection site involved a putaminal sector rostral to the motor putamen as usually defined. The distribution of the labeling involving the ventral premotor area F5, frontal operculum, rostral F3, ventrolateral prefrontal sectors including area 12 and ventral area 46, and inferior parietal and opercular parietal sectors suggests that the injection site involved a striatal sector related to hand and mouth motor control, at least in part corresponding to the rostral striatal target of the lateral grasping network projections (Gerbella et al., 2016). In the contralateral hemisphere, the amount of CSt labeled neurons was relatively robust, though lower than that observed for the caudate tracer injections (Table 3). Specifically, labeled CSt cells were mostly equally distributed between the rostral cingulate and premotor cortex and only marginally involved prefrontal and caudal cingulate cortex. Again, parietal and temporal cortex, but also the insula, were virtually devoid of labeling. The areal distribution of the labeling (Fig. 8) shows that the ratio of labeled CSt cells in the contra- vs. ipsilateral cortical areas was quite low for F5 and frontal operculum and relatively high for the rostral cingulate areas and premotor areas F6 and F7. Contralateral area 24c/d was among the five most labeled areas, considering ipsilateral and contralateral areas.

In Case 75r CTBg, the injection site was placed in the dorsal part of the putamen at about the level of the AC (Fig. 1). In the ipsilateral hemisphere (Fig. 9) labeled CSt cells were mostly concentrated in the frontal and cingulate motor cortex. As expected from the somatotopy of the motor putamen (Alexander and DeLong, 1985), in the frontal motor cortex labeled cells were

densest in the medial part of F1 and in the caudal half of F3 suggesting that the injection site involved the leg/trunk representation. Additional weaker labeling was observed in dorsomedial SI, in the superior parietal area PE, and in the caudal cingulate cortex. In the contralateral hemisphere labelled CSt cells were about 22% of the total ipsi- + contralateral labeling and were observed almost completely in the frontal motor cortex, mainly in F1, F3, and F2, and in area 24c/d, except for some weak labeling in the parietal cortex (mostly in SI) and in the caudal cingulate cortex. As observed in other cases, out of the five most labeled cortical areas, two were in the contralateral hemisphere (Fig. 8). Furthermore, based on the number of labeled cells, about 1/3 of the overall input to the injected striatal zone from areas 24c/d, F3, and F2 originated from the contralateral hemisphere (nearly 1/5 from contralateral F1).

Three tracer injections were placed more ventrally in the motor putamen at different rostrocaudal levels (Fig. 1). In Case 71r DY the injection site was located in the middle of the motor putamen and was much smaller than expected, likely because the volume of tracer injected was smaller than planned. In Cases 77l CTBg and 71l FB, the injections were located slightly more caudal and ventral. In all these cases, the labeling in the ipsilateral hemisphere was mostly located in the frontal and cingulate motor cortex, but about 15-20% of the labeled cells were in the parietal cortex (Table 2). As expected from the somatotopy of the motor putamen (Alexander and DeLong, 1985), the labeling involved in all cases the middle part of F1 and F3 and ventral premotor areas F5 and F4, suggesting involvement by the injection sites of the arm/hand representation (Figs. 8, 10 and 11). In Cases 77l CTBg and 71l FB the labeling extended also more ventrally in F1 and in F5, more rostrally in F3 and in the frontal operculum, suggesting an involvement also of the face/mouth representation. In the parietal cortex the most labeled areas were SI, SII, and PE and rostral inferior parietal areas. In the contralateral hemisphere, the number of labeled cells (5-12%) was considerably lower than that observed after the other putaminal and the caudate injections (Table 3). However, this labeling involved a limited number of contralateral areas (Fig. 2), so that the relative contribution of the crossed projections to the whole input from areas 24c/d, F3, and F1 was about

10-20%. Interestingly, in Cases 71l FB and 77l CTBg the contralateral labeling tended to be densest in rostral F3 and in Case 71l FB in the lateral part of the ventral premotor cortex, likely involving preferentially face/mouth fields. Furthermore, except for some sparse labeling located in SI (also SII in Case 71r DY), the contralateral parietal labeling was negligible, even if in these three cases the ipsilateral parietal cortex hosted 13-19% of the overall labeled cells.

Laterality of CSt projections

Our data showed that the relative balance of ipsilateral and contralateral projections from frontal and cingulate areas varied widely. Accordingly, we examined whether the proportion of contralateral CSt projections (i.e., contralaterality index = contralateral cells in area X/ipsi + contra cells in area X) in each cortical area was related to the total amount of ipsi+ contralateral labeling in that area (Figure 12). This analysis did not show a correlation between the contralaterality index and total labeling across cortical areas (r=0,27). Rather, the cortical areas with the largest projections to a striatal injection site could have either high (>0,3; area 24/32 after caudate head injections) or low contralaterality indexes (F5 and F1 after mid-ventral motor putamen injections). Similarly, other areas (F6, F7, and FrOp) with moderate projections (< 5%) also exhibited a relatively high contralaterality index in some cases and a low contralaterality index in other cases. Furthermore, in several cases, the contralaterality index of the CSt projections appears to vary according to the target striatal zone. For example, area 24c/d exhibited a relatively high contralaterality index for the projections to the caudate and a lower one for the projections to the putamen, independently from the strength of its projections. Among the frontal motor areas, F3 showed a relatively high contralaterality index for the projections to the caudate body and dorsal motor putamen and a lower one for the projections to the mid-ventral motor putamen, again independently from the strength of its projections. Finally, F1 had a higher contralaterality index for its projections to the leg/trunk-related motor putamen and a quite low one for the projections to the hand-related motor putamen.

DISCUSSION

The present study provides a detailed description of the origin and strength of striatal input from the ipsilateral and contralateral (crossed CSt projections) hemispheres in the non-human primate. As has been noted over the last 50 years, striatal input is dominated by the ipsilateral cortex, but our results now demonstrate that a substantial amount originates from the contralateral cortex. Whereas ipsilateral projections originate from cingulate, frontal, parietal, insular, and temporal cortex, crossed CSt projections originate almost exclusively from cingulate, prefrontal, and frontal motor areas. In some cases, the contribution of contralateral cingulate and frontal areas is quite high and even equal to that from the same area of the ipsilateral hemisphere. The crossed CSt projections from the primary motor cortex tend to be relatively robust for the leg/trunk representation and weak for the hand representation. Overall, the distribution of crossed CSt projections suggests that they may provide a substrate for bilateral integration of motor, motivational, and cognitive signals during behavior.

Accordingly, the present study highlights that crossed CSt projections could be an important variable to consider in defining the pattern of information convergence in the striatum.

Crossed CSt projections

Crossed CSt projections have been first noted in the rabbit, cat, and rat (Carman 1965) and then in the macaque (Kemp and Powell, 1970; Fallon and Ziegler, 1979) based on degenerative changes in the striatum after cortical lesions. Crossed CSt projections have been then described in the macaque after neural tracer injections in the primary motor and premotor (Kunzle, 1975; 1978; Liles and Updyke, 1985; Huerta and Kaas, 1990; Parthasarathy et al. 1992), prefrontal (McGuire et al., 1991), and parietal (Cavada and Goldman-Rakic, 1991) cortex. These studies, based on anterograde tracer injections at the cortical level could not give a comprehensive picture of the origin of the crossed CSt projections to a given striatal sector and an estimate of the weight of these projections compared to the direct ones. At our knowledge, only Jones et al. (1977) provided a qualitative description of crossed CSt projections based on injections of a retrograde tracer in the

motor putamen in the squirrel monkey. As Jones et al. (1977), after injections in the motor putamen we found an almost symmetrical distribution of labeled CSt cells in the ipsi vs contralateral frontal cortex and a virtual absence of labeled CSt cells in the contralateral parietal cortex. The very poor or even absent labeling observed in the contralateral parietal cortex in all the cases of the present study, including those in which labeling in the ipsilateral parietal cortex was quite robust, is in apparent discrepancy with the observations of Cavada and Goldman-Rakic (1991) after very large tracer injections in different parietal areas. It is possible that CSt parietal cells are relatively few and sparsely project to the striatum so that they are very difficult to be labeled after restricted injections of retrograde tracers in the striatum. On the other hand, as in the present study, Griggs et al. (2017) showed contralateral labeling in the frontal and cingulate, but not in the parietal, temporal, and insular cortex after tracer injections in the caudate head or tail.

The present observations that the crossed CSt projections in the macaque originate predominantly from frontal and cingulate areas are in good agreement with the results of McGuire et al. (1991) and Innocenti et al. (2017), based on tracer injections at cortical level. Specifically, McGuire et al. (1991) noted that some areas (e.g. area 46) display relatively weak crossed projections, whereas other areas (e.g., F3-SMA proper) appear to project almost equally to both ipsi- and contralateral striatum. In this context, it could be worth noting that in the present data there were some areas that were always sources of relatively weak "additional" projections, in most cases showing a relatively high contralaterality index. It is possible that in our cases the target striatal zones of these areas have been only marginally involved. However, it could be also that some areas tend to have sparse and diffuse bilateral CSt projections.

Crossed CSt projections may also be present in the human brain. Based on tractographic data, Innocenti et al. (2017) found that as in macaques crossed CSt projections in humans originate predominantly from frontal areas, but also from parietal regions of the superior and inferior parietal lobule and from the superior temporal gyrus. The presence in humans of crossed CSt projections from specific posterior parietal regions is supported by functional connectivity data (Jarbo and

Verstynen, 2015). Neurodevelopmental studies showed that in mice soon after birth crossed CSt projections originate from almost the entire hemisphere, whereas after two weeks mainly from frontal and cingulate areas possibly because of either retraction of initial collaterals to the contralateral striatum, or death of an early developmental population of CSt neurons (Sohur et al., 2014). Accordingly, the presence of crossed CSt projections from parietal and temporal areas in humans, but not in macaques could be accounted for by a differential maturation of these projections across different species.

Functional considerations

Early models of CSt projections in non-human primates have favored a modular organization of the striatum in which different striatal zones are targets of specific cortical regions (Alexander et al., 1986) and, in turn, are at the origin of largely segregated basal ganglia-thalamo-cortical loops (Middelton and Strick, 2000; Kelly and Strick, 2004). Subsequent studies have revealed a higher level of complexity of the corticostriatal projections topography. First, the cortical input to a specific striatal zone originates not only from a limited set of closely related neighbor areas, as initially described (Takada et al., 1998; Nambu 2011; Averbeck et al., 2014), but also from distant, interconnected areas jointly involved in large-scale functionally specialized cortical networks (Gerbella et al., 2016; Choi et al., 2017). Second, the different striatal zones are targets of characteristically weighted laminar projections from multiple input areas (Griggs et al., 2017; Borra et al., 2021). Finally, the present data suggest that information processing in the striatum can also rely on substantial input from the contralateral hemisphere.

As crossed CSt projections in the macaque brain have been so far poorly considered, their possible contribution to information processing in the striatum still remains to be defined. These projections could indeed provide a substrate for interhemispheric transfer of signals in parallel to the callosal connectivity. Based on conduction delay estimations, it has been suggested that crossed CSt projections mediate a transfer of information considerably faster than through the callosal connectivity (Innocenti et al., 2017). Furthermore, whereas callosal projections connect almost

entirely the two hemispheres (see, e.g., Innocenti et al., 2021), crossed CSt projections originates mostly from frontal and cingulate areas, suggesting a role more focused on motor control or/and executive functions. In this context, crossed CSt projections could provide the substrate for bilateral diffusion of motor, motivational, and cognitive signals necessary for reinforcement learning and selection of those actions or action sequences which are most appropriate for achieving a behavioral goal (see, Averbeck and O'Doherty, 2022) and for inhibitory control of impulsive motor behavior (Oguchi et al., 2021). Furthermore, in the motor putamen, crossed CSt projections could have a role in controlling actions or action sequences involving both sides of the body.

Indeed, brain imaging evidence in humans showed bilateral activation in the motor putamen during the execution of unilateral simple foot, hand, and mouth movements (e.g., Gerardin et al., 2003). Interestingly, in the left putamen the activation foci for the right or left hand movements appeared largely segregated (Gerardin et al., 2003), resembling the segregation between the terminal fields of direct and crossed CSt projections to the striatal hand representation in the squirrel monkey (Flaherty and Graybiel, 1993). Furthermore, bilateral activation of the striatum has been observed during the execution of right hand finger-tapping tasks with increasing degrees of complexity (Lehericy et al., 2006; Bednark et al., 2015). The observed striatal activation foci tended to shift progressively more rostrally with the increase in complexity or frequency of the task execution (Lehericy et al., 2006). Finally, bilateral striatal activation has been observed during early phases of visuomotor adaptation of arm movements (Seidler et al., 2006) and, especially in the anterior striatum during the encoding of novel working memory items (Geiger et al., 2018)

According to Wymbs et al. (2012) bilateral putamen activity is necessary for the strengthening of motor-motor associations at the basis of action chunking processes. Chunking in motor sequencing is considered a key function of the basal ganglia and allows groups of individual movements to be prepared and executed as a single motor program facilitating learning and performance of complex sequences (Halford et al., 1998).

433 Crossed CSt projections could play a potentially important role in behavioral compensation after
434 brain lesions. Specifically, these projections could have a role in compensatory relearning of motor
435 strategies in the context of the reorganization mechanisms of the motor system occurring after
436 cortical stroke (Balbinot and Pedrini Schuch, 2019). In support of this proposal, there is evidence in
437 rodents for axonal sprouting of crossed CSt projections and neurochemical signs of increased cell
438 activity in the denervated striatum after sensorimotor cortex lesions (Napieralski et al., 1996; Cheng
439 et al., 1998; Uryu et al., 2001). The presence in macaques of crossed CSt projections that appear
440 even stronger than in rodents is an incentive for experimental studies in non-human primates and
441 clinical studies in neurological patients focused on the role of these projections in compensatory
442 mechanisms after stroke.
443

444 **REFERENCES**

445 Alexander GE, DeLong MR, Strick PL. 1986. Parallel organization of functionally segregated
446 circuits linking basal ganglia and cortex. Annu Rev Neurosci 9:357–381.

447 Alexander GE, DeLong MR. 1985. Microstimulation of the primate neostriatum: II. Somatotopic
448 organization of striatal microexcitable zones and their relation to neuronal response properties. J
449 Neurophysiol 53:1417–1430.

450 Averbeck BB, Lehman J, Jacobson M, Haber SN. 2014. Estimates of projection overlap and
451 zones of convergence within frontal-striatal circuits. J Neurosci. 34:9497-505. doi:
452 10.1523/JNEUROSCI.5806-12.2014.

453 Averbeck B, O'Doherty JP. 2022. Reinforcement-learning in fronto-striatal circuits.
454 Neuropsychopharmacology. 47:147-162. doi: 10.1038/s41386-021-01108-0.

455 Balbinot G, Schuch CP. 2019. Compensatory relearning following stroke: cellular and plasticity
456 mechanisms in rodents. Front Neurosci. 12:1023. doi: 10.3389/fnins.2018.01023.

457 Bednark JG, Campbell ME, Cunnington R. 2015. Basal ganglia and cortical networks for
458 sequential ordering and rhythm of complex movements. Front Hum Neurosci. 9:421. doi:
459 10.3389/fnhum.2015.00421.

460 Belmalih A, Borra E, Contini M, Gerbella M, Rozzi S, Luppino G. 2009. Multimodal
461 architectonic subdivision of the rostral part (area F5) of the macaque ventral premotor cortex. J
462 Comp Neurol. 512:183–217.

463 Borra E, Belmalih A, Calzavara R, Gerbella M, Murata A, Rozzi S, Luppino G. 2008. Cortical
464 connections of the macaque anterior intraparietal (AIP) area. Cereb Cortex. 18:1094–1111.

465 Borra E, Gerbella M, Rozzi S, Luppino G. 2017. The macaque lateral grasping network: A
466 neural substrate for generating purposeful hand actions. Neurosci Biobehav Rev. 75:65-90. doi:
467 10.1016/j.neubiorev.2017.01.017.

Borra E, Rizzo M, Gerbella M, Rozzi S, Luppino G. 2021. Laminar origin of corticostriatal projections to the motor putamen in the macaque brain. J Neurosci. 41:1455-1469. doi: 10.1523/JNEUROSCI.1475-20.2020.

Boussaoud D, Ungerleider LG, Desimone R. 1990. Pathway for motion analysis: cortical connections of the medial superior temporal and fundus of the superior temporal visual areas in the macaque. J Comp Neurol. 296:462–495.

Caminiti R, Borra E, Visco-Comandini F, Battaglia-Mayer A, Averbeck BB, Luppino G. 2017. Computational architecture of the parieto-frontal network underlying cognitive-motor control in monkeys. eNeuro. 4(1):ENEURO.0306-16.2017. doi: 10.1523/ENEURO.0306-16.2017.

Carman JB, Cowan WM, Powell TP, Webster KE.1965. A bilateral cortico-striate projection. J Neurol Neurosurg Psychiatry. 28:71-7. doi: 10.1136/jnnp.28.1.71.

Carmichael ST, Price JL. 1994. Architectonic subdivision of the orbital and medial prefrontal cortex in the macaque monkey. J Comp Neurol. 346:366–402.

Cavada C, Goldman-Rakic PS. 1991. Topographic segregation of corticostriatal projections from posterior parietal subdivisions in the macaque monkey. Neuroscience. 42:683-96. doi: 10.1016/0306-4522(91)90037-o.

Cheng HW, Tong J, McNeill TH. 1998. Lesion-induced axon sprouting in the deafferented striatum of adult rat. Neurosci Lett. 242:69-72. doi: 10.1016/s0304-3940(98)00050-0.

Choi EY, Tanimura Y, Vage PR, Yates EH, Haber SN. 2017. Convergence of prefrontal and parietal anatomical projections in a connectional hub in the striatum. Neuroimage. 146:821-832. doi: 10.1016/j.neuroimage.2016.09.037.

Demelio S, Bettio F, Gobbetti E, Luppino G. 2001. Threedimensional reconstruction and visualization of the cerebral cortex in primates. In: Ebert D, Favre J, Peikert R, editors. Data visualization 2001. New York, NY, USA: Springer Verlag. p. 147–156.

Fallon JH, Ziegler BT. 1979 The crossed cortico-caudate projection in the rhesus monkey. Neurosci Lett 29-32. doi: 10.1016/0304-3940(79)91524-6. DOI: 10.1016/0304-3940(79)91524-6

494 Flaherty AW, Graybiel AM. 1993. Two input systems for body representations in the primate
495 striatal matrix: experimental evidence in the squirrel monkey. J Neurosci. 13:1120-37. doi:
496 10.1523/JNEUROSCI.13-03-01120.1993.
497 Geiger LS, Moessnang C, Schäfer A, Zang Z, Zangl M, Cao H, van Raalten TR, Meyer-
498 Lindenberg A, Tost H. 2018. Novelty modulates human striatal activation and prefrontal-striatal
499 effective connectivity during working memory encoding. Brain Struct Funct. 223:3121-3132. doi:
500 10.1007/s00429-018-1679-0.
501 Gerardin E, Lehéricy S, Pochon JB, Tézenas du Montcel S, Mangin JF, Poupon F, Agid Y, Le
502 Bihan D, Marsault C. 2003. Foot, hand, face and eye representation in the human striatum. Cereb
503 Cortex. 13:162-9. doi: 10.1093/cercor/13.2.162.
504 Gerbella M, Belmalih A, Borra E, Rozzi S, Luppino G. 2007. Multimodal architectonic
505 subdivision of the caudal ventrolateral prefrontal cortex of the macaque monkey. Brain Struct
506 Funct. 212:269–301.
507 Gerbella M, Borra E, Mangiaracina C, Rozzi S, Luppino G. 2016. Corticostriate projections from
508 areas of the “lateral grasping network”: evidence for multiple hand-related input channels. Cereb
509 Cortex 26:3096–3078.
510 Gregoriou GG, Borra E, Matelli M, Luppino G. 2006. Architectonic organization of the inferior
511 parietal convexity of the macaque monkey. J Comp Neurol. 496:422–451.
512 Griggs WS, Kim HF, Ghazizadeh A, Costello MG, Wall KM, Hikosaka O. 2017. Flexible and
513 stable value coding areas in caudate head and tail receive anatomically distinct cortical and
514 subcortical inputs. Front Neuroanat. 11:106. doi: 10.3389/fnana.2017.00106. eCollection 2017.
515 Halford GS, Wilson WH, Phillips S. 1998. Processing capacity defined by relational complexity:
516 implications for comparative, developmental, and cognitive psychology. Behav. Brain Sci.21, 803–
517 831, discussion 831–864.

518 Huerta MF, Kaas. JH. 1990. Supplementary eye field as defined by intracortical
519 microstimulation: connections in macaques. J Comp Neurol 293:299-330. doi:
520 10.1002/cne.902930211.
521 Innocenti GM, Dyrby TB, Andersen KW, Rouiller EM, Caminiti R. 2017. The crossed
522 projection to the striatum in two species of monkey and in humans: behavioral and evolutionary
523 significance. Cereb Cortex. 27:3217-3230. doi: 10.1093/cercor/bhw161.
524 Innocenti GM, Schmidt K, Milleret C, Fabri M, Knyazeva MG, Battaglia-Mayer A, Aboitiz F,
525 Ptito M, Caleo M, Marzi CA, Barakovic M, Lepore F, Caminiti R. 2021. The functional
526 characterization of callosal connections. Prog Neurobiol. 208:102186. doi:
527 10.1016/j.pneurobio.2021.102186.
528 Jarbo K, Verstynen TD. 2015. Converging structural and functional connectivity of orbitofrontal,
529 dorsolateral prefrontal, and posterior parietal cortex in the human striatum. J Neurosci. 35:3865-78.
530 doi: 10.1523/JNEUROSCI.2636-14.2015.
531 Jones EG, Coulter JD, Burton H, Porter R. 1977. Cells of origin and terminal distribution of
532 corticostriatal fibers arising in the sensory-motor cortex of monkeys. J Comp Neurol. 173:53-80.
533 doi: 10.1002/cne.901730105.
534 Kaas JH, Hackett TA. 2000. Subdivisions of auditory cortex and processing streams in primates.
535 Proc Natl Acad Sci USA. 97: 11793–11799.
536 Kelly RM, Strick PL. 2004. Macro-architecture of basal ganglia loops with the cerebral cortex:
537 use of rabies virus to reveal multisynaptic circuits. Prog Brain Res. 143:449-59. doi:
538 10.1016/s0079-6123(03)43042-2.
539 Kemp JM, Powell TP. 1970. The cortico-striate projection in the monkey. Brain. 93:525-46. doi:
540 10.1093/brain/93.3.525.
541 Künzle H. 1975. Bilateral projections from precentral motor cortex to the putamen and other
542 parts of the basal ganglia. An autoradiographic study in Macaca fascicularis. Brain Res. 88:195-
543 209. doi: 10.1016/0006-8993(75)90384-4.

544 Künzle H. 1978. An autoradiographic analysis of the efferent connections from premotor and
545 adjacent prefrontal regions (areas 6 and 9) in macaca fascicularis. Brain Behav Evol. 15:185-234.
546 doi: 10.1159/000123779.
547 Lehéricy S, Bardinet E, Tremblay L, Van de Moortele PF, Pochon JB, Dormont D, Kim DS,
548 Yelnik J, Ugurbil K. 2006. Motor control in basal ganglia circuits using fMRI and brain atlas
549 approaches. Cereb Cortex. 16:149-61. doi: 10.1093/cercor/bhi089.
550 Liles SL, Updyke BV. 1985. Projection of the digit and wrist area of precentral gyrus to the
551 putamen: relation between topography and physiological properties of neurons in the putamen.
552 Brain Res. 339:245-55. doi: 10.1016/0006-8993(85)90089-7
553 Luppino G, Ben Hamed S, Gamberini M, Matelli M, Galletti C. 2005. Occipital (V6) and
554 parietal (V6A) areas in the anterior wall of the parieto-occipital sulcus of the macaque: a
555 cytoarchitectonic study. Eur J Neurosci. 21:3056–3076.
556 Matelli M, Luppino G, Rizzolatti G. 1985. Patterns of cytochrome oxidase activity in the frontal
557 agranular cortex of the macaque monkey. Behav Brain Res. 18:125–136.
558 Matelli M, Luppino G, Rizzolatti G. 1991. Architecture of superior and mesial area 6 and the
559 adjacent cingulate cortex in the macaque monkey. J Comp Neurol. 311:445–462.
560 McGuire PK, Bates JF, Goldman-Rakic PS. 1991. Interhemispheric integration: II. Symmetry
561 and convergence of the corticostriatal projections of the left and the right principal sulcus (PS) and
562 the left and the right supplementary motor area (SMA) of the rhesus monkey. Cereb Cortex. 1:408-
563 17. doi: 10.1093/cercor/1.5.408.
564 Middleton FA, Strick PL. 2000. Basal ganglia and cerebellar loops: motor and cognitive circuits.
565 Brain Res Brain Res Rev 31:236–250.
566 Morecraft RJ, Cipolloni PB, Stilwell-Morecraft KS, Gedney MT, Pandya DN. 2004.
567 Cytoarchitecture and cortical connections of the posterior cingulate and adjacent somatosensory
568 fields in the rhesus monkey. J Comp Neurol. 469:37–69.
569 Nambu A. 2011. Somatotopic organization of the primate basal ganglia. Front Neuroanat 5:26.

570 Napieralski JA, Butler AK, Chesselet MF. 1996. Anatomical and functional evidence for lesion-
571 specific sprouting of corticostriatal input in the adult rat. J. Comp. Neurol. 373, 484–497. doi:
572 10.1002/(SICI)1096-9861(19960930)373:4<484::AID-CNE2>3.0.CO;2-Y
573 Oguchi M, Tanaka S, Pan X, Kikusui T, Moriya-Ito K, Kato S, Kobayashi K, Sakagami M.
574 2021. Chemogenetic inactivation reveals the inhibitory control function of the prefronto-striatal
575 pathway in the macaque brain. Commun Biol. 4:1088. doi: 10.1038/s42003-021-02623-y.
576 Pandya DN, Seltzer B. 1982. Intrinsic connections and architectonics of posterior parietal cortex
577 in the rhesus monkey. J Comp Neurol. 204:196–210.
578 Parthasarathy HB, Schall JD, Graybiel AM. 1992. Distributed but convergent ordering of
579 corticostriatal projections: analysis of the frontal eye field and the supplementary eye field in the
580 macaque monkey. J Neurosci. 12:4468-88. doi: 10.1523/JNEUROSCI.12-11-04468.1992.
581 Saleem KS, Kondo H, Price JL. 2008. Complementary circuits connecting the orbital and medial
582 prefrontal networks with the temporal, insular, and opercular cortex in the macaque monkey. J
583 Comp Neurol. 506:659–693.
584 Saleem KS, Logothetis NK. 2012. A combined MRI and histology atlas of the rhesus monkey
585 brain in stereotaxic coordinates. In: With horizontal, coronal, and sagittal series. 2nd ed. San Diego:
586 Academic Press/Elsevier.
587 Saleem KS, Miller B, Price JL. 2014. Subdivisions and connectional networks of the lateral
588 prefrontal cortex in the macaque monkey. J Comp Neurol. 522:1641–1690.
589 Seidler RD, Noll DC, Chintalapati P. 2006. Bilateral basal ganglia activation associated with
590 sensorimotor adaptation. Exp Brain Res. 175:544-55. doi: 10.1007/s00221-006-0571-y.
591 Sohur US, Padmanabhan HK, Kotchetkov IS, Menezes JR, Macklis JD. 2014. Anatomic and
592 molecular development of corticostriatal projection neurons in mice. Cereb Cortex. 24:293-303.
593 doi: 10.1093/cercor/bhs342.
594

595 Strick PL, Dum RP, Picard N. 1995. Macro-organization of the circuits connecting the basal
596 ganglia with the cortical motor areas. In: Models of information processing in the basal ganglia
597 (Houk G, ed), pp 117–130. Cambridge, MA:MIT Press.
598 Takada M, Tokuno H, Nambu A, Inase M. 1998. Corticostriatal input zones from the
599 supplementary motor area overlap those from the contra- rather than ipsilateral primary motor
600 cortex. Brain Res. 791:335-40. doi: 10.1016/s0006-8993(98)00198-x.
601 Uryu K, MacKenzie L, Chesselet MF. 2001. Ultrastructural evidencefor differential axonal
602 sprouting in the striatum after thermocoagulatory and aspiration lesions of the cerebral cortex in
603 adult rats. Neuroscience 105, 307–316. doi: 10.1016/S0306-4522(01)00203-2
604 Wymbs NF, Bassett DS, Mucha PJ, Porter MA, Grafton ST. 2012. Differential recruitment of the
605 sensorimotor putamen and frontoparietal cortex during motor chunking in humans. Neuron 74, 936–
606 946. doi: 10.1016/j.neuron.2012.03.038
607

608 **Table 1.** Animals used, location of injection sites, and type and amount of injected tracers

609

Case	Sex	Age	Weight	Hemisphere	Location	AP*	Tracer	Amount	Survival time
71	F	6.5	3.3	L	Putamen	-2	FB 3%	1 X 0.3 µl	28 days
				R	Putamen	-1	DY 2%	1 X 0.3 µl**	21 days
75	M	6	3.5	L	Caudate	+6	LYD 10%	1 X 1 µl	28 days
				R	Putamen	0	CTBg 1%	1 X 1 µl	21 days
					Caudate	+1	DY 2%	1 X 0.25 µl	21 days
76	M	9	15	R	Caudate	+7	WGA 4%	1 X 0.3 µl	48 hours
77	M	9	15	L	Putamen	-3	CTBg 1%	1 X 1 µl	21 days
				R	Putamen	+3	WGA 4%	1 X 0.2 µl	48 hours

610 * mm from the crossing of the anterior commissure; ** injected volume likely smaller than planned

611

612 **Table 2**. Regional distribution (%) and total number (n) of labeled cortical neurons observed in the

613 ipsilateral hemisphere, following tracer injections in the caudate and in the putamen

614

	Case	Rostral cingulate	Pref	Motor	Parietal	Insula	Temp	Caudal cingulate	Other	Total	n. cells
Caudate	75l LYD Lateral Head	21,5	37,8	8,4	6,1	4,8	13,5	7	0,9	100	42183
	76r WGA Medial Head	30,6	48,5	4,1	0,1	2,3	9,4	4,4	0,6	100	140790
	75r DY Body	7	4,8	74,1	11,5	-	-	2,6	-	100	33082
Putamen	77r WGA Rostral	23	17,5	37,8	8,1	7	4,3	2,3	-	100	99341
	75r CTBg Dorsal Motor	15,3	0,7	61,9	16,6	1,4	-	4,1	-	100	119306
	77l CTBg Middle Motor	8,3	1	64,5	21,6	2	0,8	1,8	-	100	75292
	71r DY Middle Motor	-	-	72,1	15,1	0,5	0,1	2,8	-	100	8360
	71l FB Mid-ventral Motor	2,6	0,5	75,5	18,6	1,2	0,8	0,8	-	100	36628

615

616

Table 3. Regional distribution (%) and total number (n) of labeled cortical neurons observed in both ipsilateral and contralateral hemisphere.

	Case		rostral cingulate	Pref	Motor	Parietal	Insula	Temp	caudal cingulate	Other	Total
Caudate	**75l LYD** Lateral Head n = 60609	Ipsi	15	26,3	5,9	5	3,3	9,3	4,9	0.6	69,6
		Contra	15,8	11,1	2,8	0,1	0,1	-	0,6	-	30,4
	76l WGA Medial Head n = 193668	Ipsi	22,2	35,3	3	0,1	1,7	6,8	3,2	0,4	72,7
		Contra	11	12,5	3,2	-	0,1	-	0,5	-	27,3
	75r DY Body n = 46626	Ipsi	5	3,4	52,6	8,1	-	-	1,8	-	70,9
		Contra	3,6	1,1	23,9	-	-	-	0,5	-	29,1
Putamen	**77l WGA** Rostral n =119738	Ipsi	19	14,5	31,3	6,7	5,8	3,5	1,9	-	82,7
		Contra	7,9	1,9	7	-	0,1	-	0,4	-	17,3
	75r CTBg Dorsal Motor n = 154075	Ipsi	11,8	0,5	47,8	13	1,2	-	3,2	-	77,5
		Contra	6,6	0,1	14,6	0,5	-	-	0,7	-	22,5
	77l CTBg Middle Motor n = 85579	Ipsi	7,2	1	56,6	19,1	1,8	0,7	1,6	-	88
		Contra	2,1	0	9,6	0,1	0	0	0,2	-	12
	71r DY Middle Motor n = 9603	Ipsi	8,2	-	62,9	13,1	0,4	0,1	2,4	-	87,1
		Contra	1,7	-	9,7	1	-	-	0,5	-	12,9
	71l FB Mid-ventral Motor n = 38407	Ipsi	2,4	0,5	72	17,8	1,1	0,8	0,8	-	95,4
		Contra	0,7	0	3,8	0	0	0	0,1	-	4,6

623 **Figure legends**

624 **Figure 1**. Location of the injection sites shown in drawings of coronal sections and in brightfield
625 (for WGA and LYD injections) and epifluorescence (for CTBg, DY, and FB injections)
626 photomicrographs. In the section drawings, all injection sites except for WGA, are depicted as a
627 black zone corresponding to the core, surrounded by a grey zone, corresponding to the halo. WGA
628 injection sites are depicted as a grey zone because of the poor definition of the core vs. the halo.
629 Calibration bars shown for the section drawing and the photomicrograph of Case 75l LYD apply to
630 all section drawings and photomicrographs, respectively. Abbreviations: C=central sulcus;
631 Cd=caudate nucleus; Cg=cingulate sulcus; Cl=claustrum; GP=globus pallidus; IA=inferior arcuate
632 sulcus; L=lateral sulcus; Put=putamen; S=spur of the arcuate sulcus; SA=superior arcuate sulcus;
633 ST=superior temporal sulcus.

634 **Figure 2.** Percent areal distribution of the total retrograde labeling observed in the ipsilateral
635 hemisphere (black) compared with that of the total retrograde labeling observed in the contralateral
636 hemisphere (grey) in all the cases of the present study. In each graph, areas are ordered based on the
637 amount of ipsilateral labeling (only areas with ipsilateral labeling >1%). Superior parietal (SPL)
638 areas and inferior parietal (IPL) areas are grouped. Each panel also reports the results of the
639 statistical analysis in which the frequency distributions of the labeled CSt cells per area in the
640 ipsilateral and the contralateral hemisphere were compared (Pearson chi-square test for
641 independence). cCg= caudal cingulate cortex (areas 23, 31, 29, 30); DF=degree of freedom;
642 FrOp=frontal operculum; Ia=agranular insula; Idg=disgranular insula; Ti=inferotemporal cortex;
643 Tm=medial temporal cortex; Tp=temporal pole; Ts=superior temporal gyrus.

644 **Figure 3**. Distribution of the retrograde labeling observed after injection of WGA in the head of
645 the caudate in Case 76r. The labeling is shown in dorsolateral and medial views of the 3D
646 reconstructions of the injected (ipsilateral) and the contralateral hemisphere and in drawings of
647 coronal sections. For the sake of comparison, in this and in the subsequent figures all the 3D
648 reconstructions are shown as a right hemisphere with the injected hemisphere on the left and all

649 section drawings with the injected hemisphere on the right. Sections are shown in a rostral to caudal
650 order (a–f). The levels at which the sections were taken are shown on the 3D reconstructions of both
651 hemispheres. Each dot corresponds to one labeled neuron. Ca=calcarine fissure; IP=intraparietal
652 sulcus; LO=lateral orbital sulcus; Lu=lunate sulcus; MO=medial orbital sulcus; P=principal sulcus;
653 Th=thalamus. Other abbreviations as in Figures 1 and 2.

654 **Figure 4**. Distribution of the retrograde labeling observed after injection of LYD in the head of
655 the caudate in Case 75l. The labeling is shown in dorsolateral and medial views of the 3D
656 reconstructions of the injected (ipsilateral) and contralateral hemisphere and in drawings of coronal
657 sections. Conventions and other abbreviations as in Figures 1-3.

658 **Figure 5**. Percent distribution of the total (ipsi + contra) retrograde labeling in ipsilateral (black)
659 and contralateral (grey) areas observed after the tracer injections in the caudate. The asterisks mark
660 in each case the five most labeled areas. Abbreviations as in Figures 2.

661 **Figure 6**. Distribution of the retrograde labeling observed after injection of DY in the caudate
662 body in Case 75r. The labeling is shown in dorsolateral and medial views of the 3D reconstructions
663 of the injected (ipsilateral) and contralateral hemisphere and in drawings of coronal sections.
664 PO=parieto-occipital sulcus. Conventions and other abbreviations as in Figures 1-3.

665 **Figure 7**. Distribution of the retrograde labeling observed after injection of WGA in the pre-
666 commissural putamen in Case 77r. The labeling is shown in dorsolateral and medial views of the
667 3D reconstructions of the injected (ipsilateral) and contralateral hemisphere and in drawings of
668 coronal sections. ParOp=parietal operculum. Conventions and other abbreviations as in Figures 1-3.

669 **Figure 8**. Percent distribution of the total (ipsi + contra) retrograde labeling in the ipsilateral
670 (black) and contralateral (grey) areas observed after the tracer injections in the putamen. The
671 asterisks mark in each case the five most labeled areas. Abbreviations as in Figures 2 and 7.

672 **Figure 9**. Distribution of the retrograde labeling observed after injection of CTBg in the dorsal
673 part of the motor putamen in Case 75r. The labeling is shown in dorsolateral and medial views of

674 the 3D reconstructions of the injected (ipsilateral) and contralateral hemisphere and in drawings of
675 coronal sections. Conventions and other abbreviations as in Figures 1-3 and 7.

676 **Figure 10**. Distribution of the retrograde labeling observed after injection of CTBg in Case 77l,
677 DY in Case 71r, and FB in 71l in the mid-ventral motor putamen, shown in dorsolateral and medial
678 views of the 3D reconstructions of the injected (ipsilateral) and contralateral hemispheres.
679 Conventions and other abbreviations as in Figures 1-3.

680 **Figure 11**. Distribution of the retrograde labeling observed after injection of CTBg in Case 77l,
681 DY in Case 71r, and FB in 71l in the mid-ventral motor putamen, shown in drawings of coronal
682 sections taken at levels indicated in Figure 9. Conventions and other abbreviations as in Figures 1-3
683 and 7.

684 **Figure 12**: Contralaterality [contralateral cells in area X/(ipsi + contra cells in area X)] of CSt
685 projections from rostral cingulate and prefrontal (A), rostral premotor (B), and caudal premotor and
686 primary motor (C) areas shown in relation to the richness (percent of ipsi- + contralateral CSt cells)
687 of the labeling. Only areas in which the total (ipsi + contra) labeling was >1% are considered in the
688 graphs. Values from injections in the caudate are shown with dots, those from injections in rostral
689 and dorsal motor putamen with diamonds, and those from injections in mid-ventral motor putamen
690 with stars. In each panel, different colors identify different areas.
691

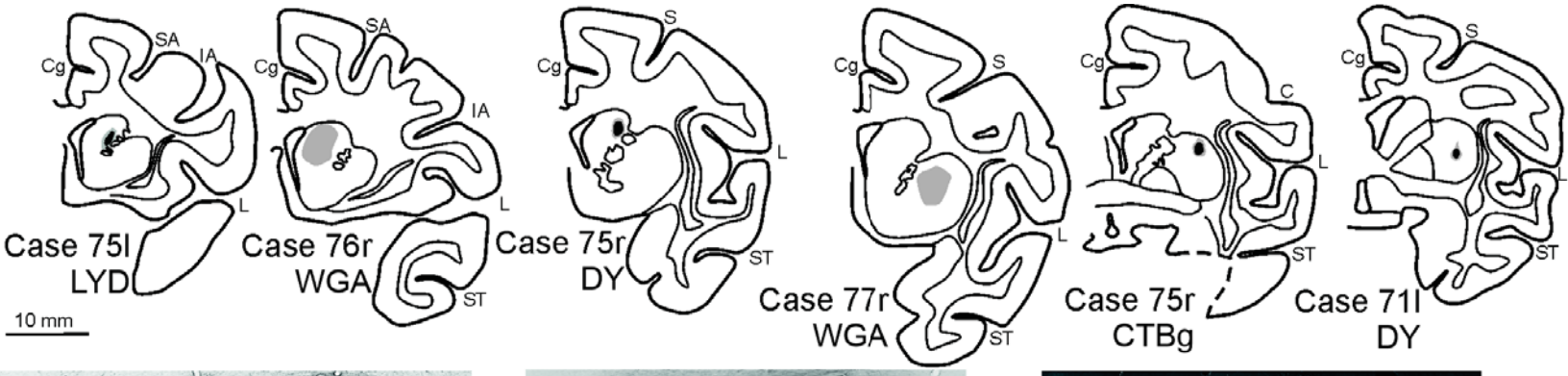
Cg
SA
IA
L
Case 75l
LYD
Case 76r
WGA
ST
S
Case 75r
DY
Case 77r
WGA
C
Case 75r
CTBg
Case 71l
DY
10 mm

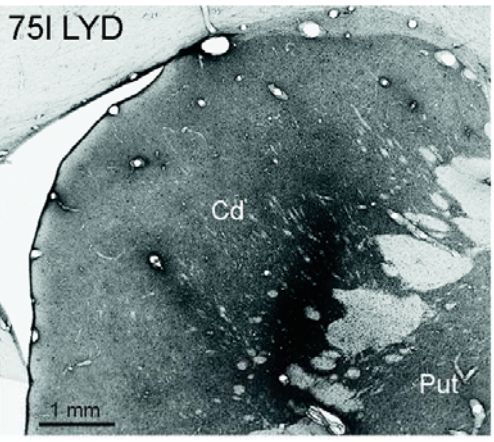
75l LYD
Cd
Put
1 mm

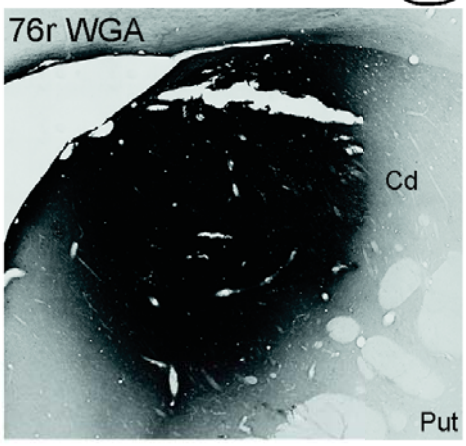
76r WGA
Cd
Put

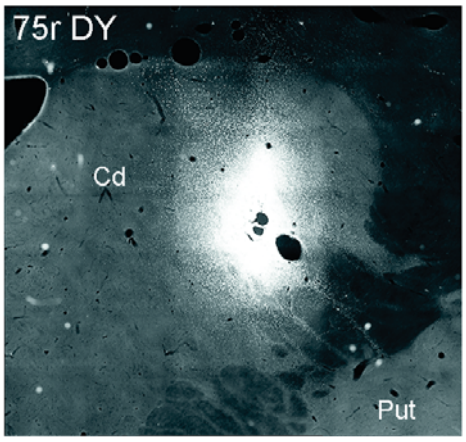
75r DY
Cd
Put

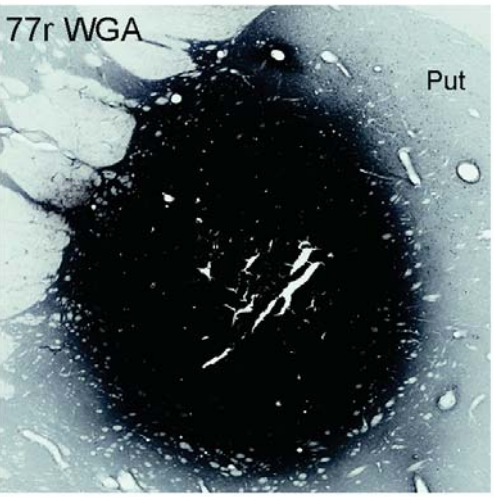
77r WGA
Put

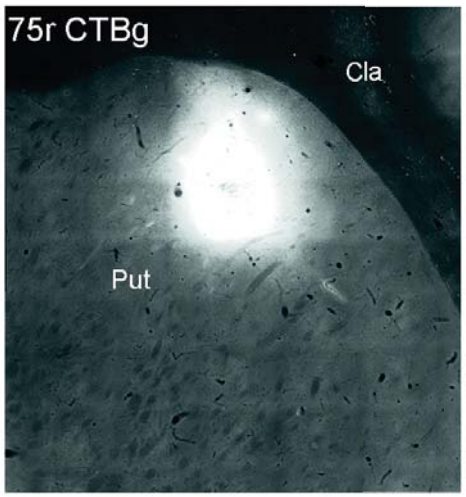
75r CTBg
Cla
Put

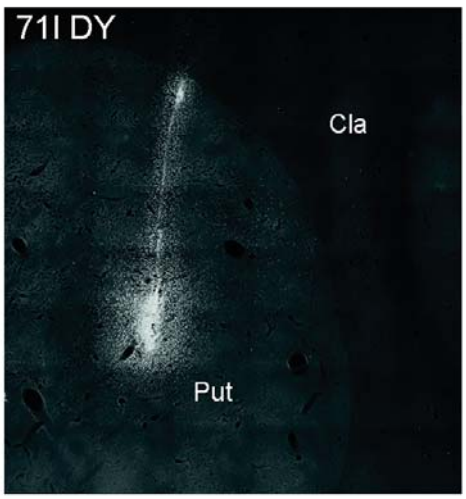
71l DY
Cla
Put

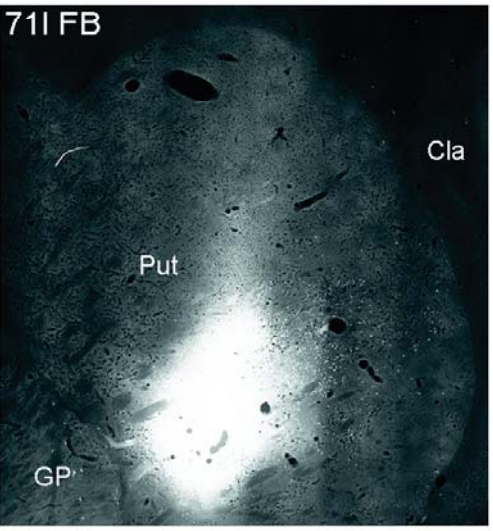
71l FB
Cla
Put
GP

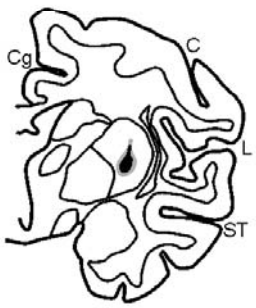
Cg
C
L
ST
Case 71l FB

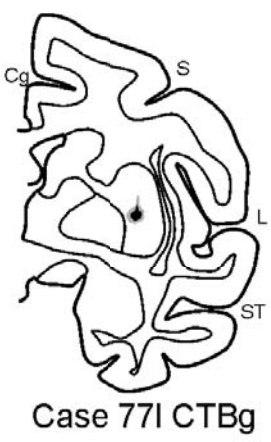
Cg
S
L
ST
Case 77l CTBg

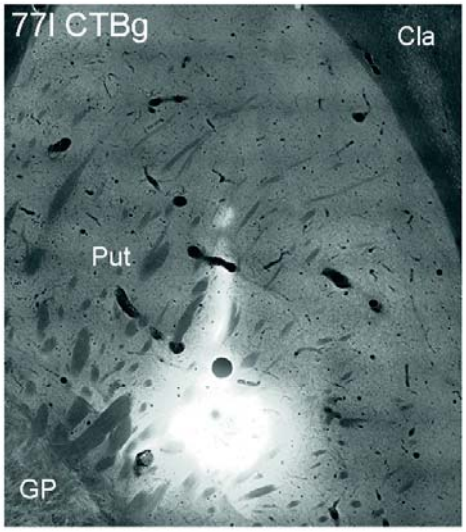
77l CTBg
Cla
Put
GP

Caudate injections

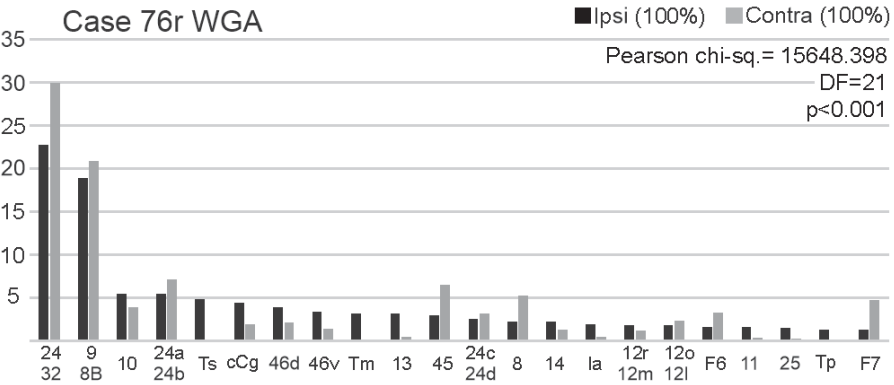

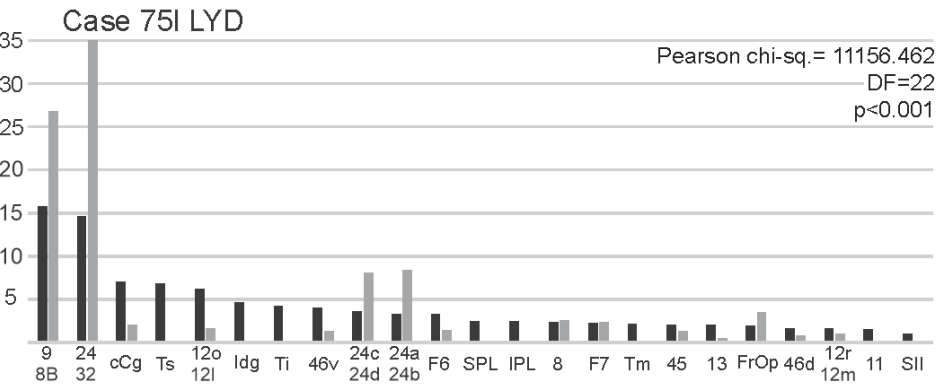

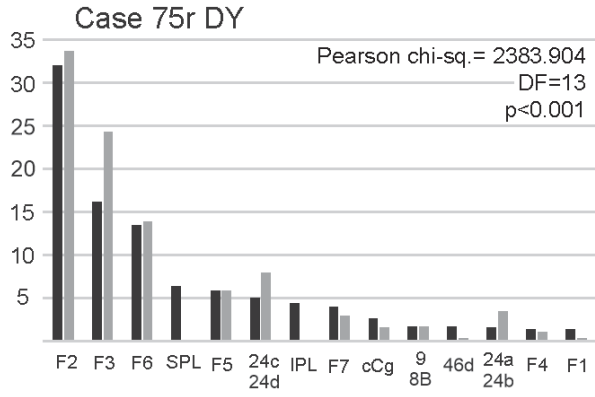

Putamen injections

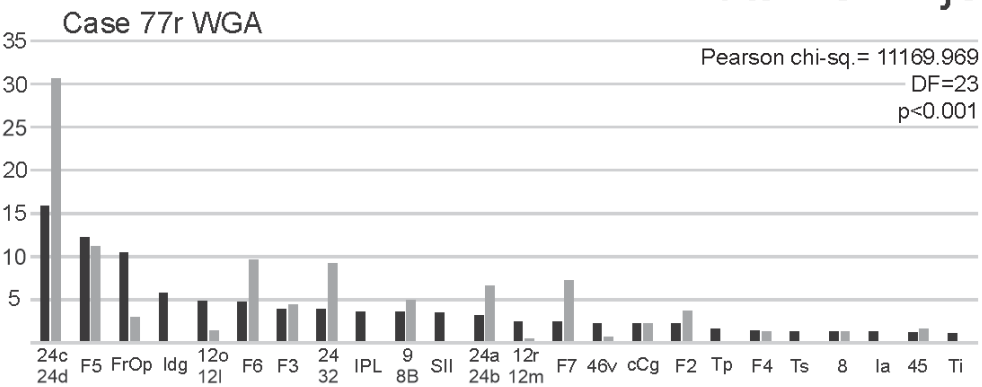

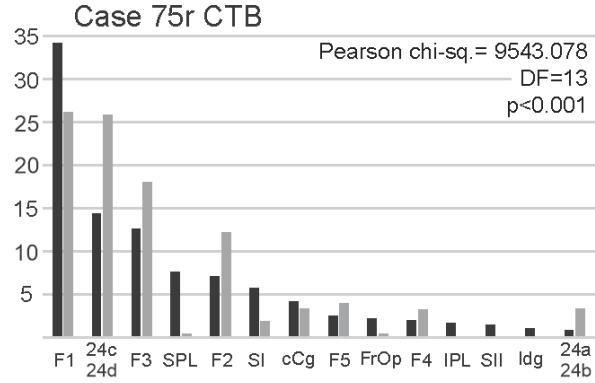

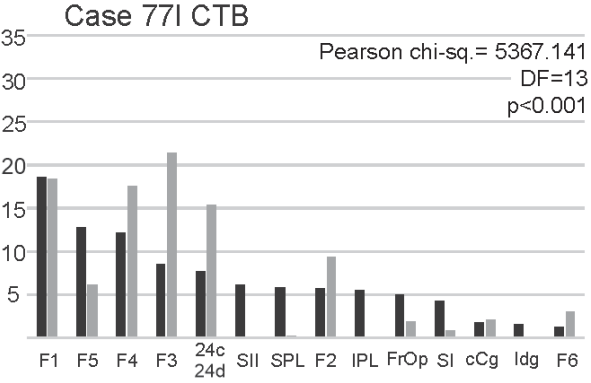

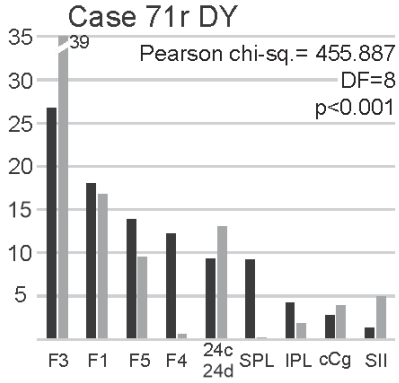

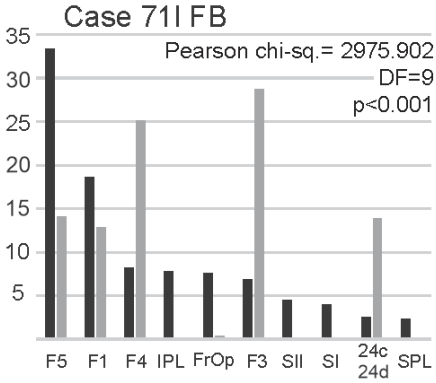

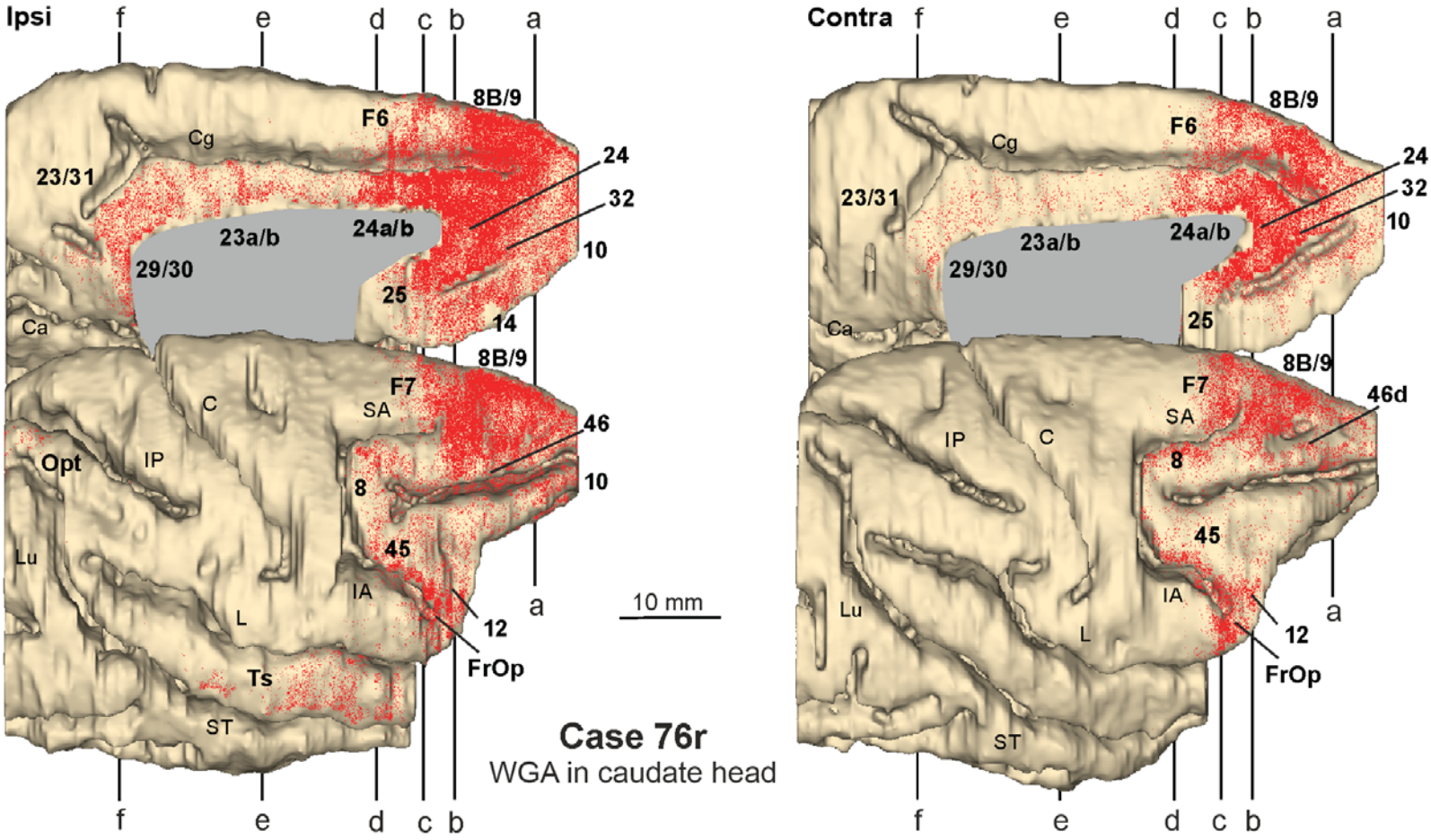
Ipsi
Contra
f
e
d
c
b
a
8B/9
F6
Cg
24
32
10
23/31
23a/b
24a/b
29/30
25
Ca
14
F7
SA
46
46d
C
IP
Opt
8
45
Lu
IA
L
12
FrOp
Ts
ST
10 mm
Case 76r
WGA in caudate head

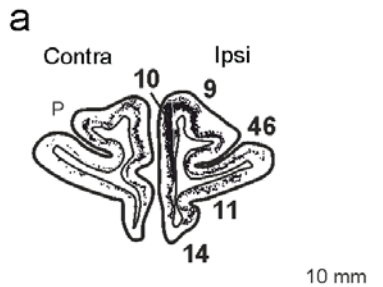
a
Contra
Ipsi
10
9
P
46
11
14
10 mm

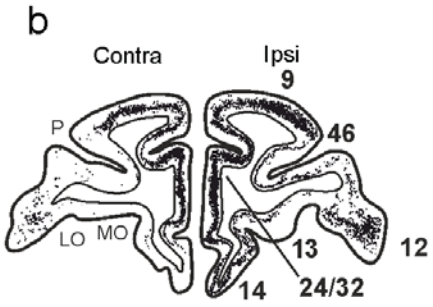
b
Contra
Ipsi
9
P
46
LO
MO
13
12
14
24/32

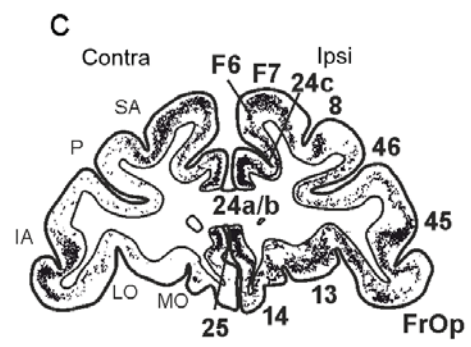
c
Contra
F6
F7
Ipsi
24c
SA
8
P
46
24a/b
IA
45
LO
MO
13
25
14
FrOp

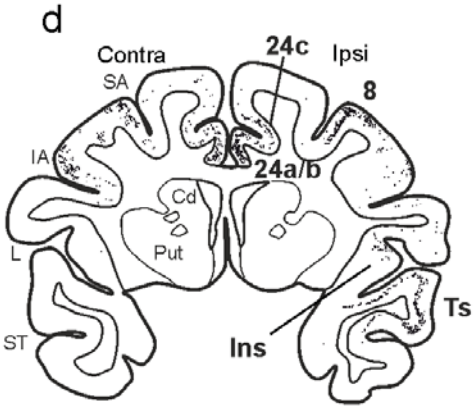
d
Contra
24c
Ipsi
SA
8
IA
24a/b
Cd
Put
L
ST
Ins
Ts

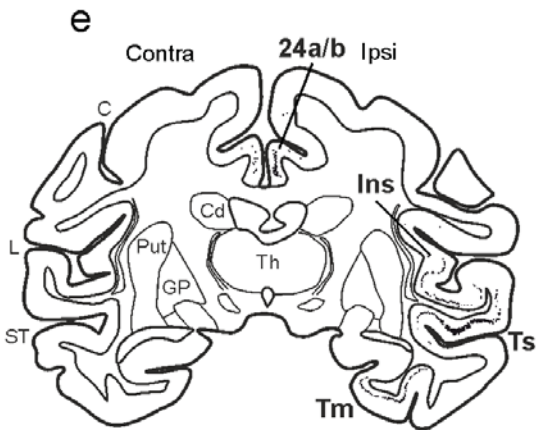
e
Contra
24a/b
Ipsi
C
Ins
Cd
L
Put
Th
GP
ST
Ts
Tm

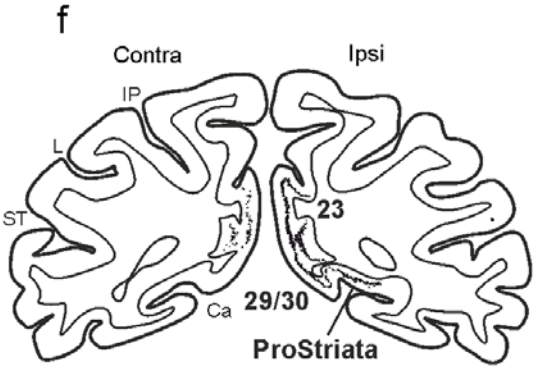
f
Contra
Ipsi
IP
L
ST
23
Ca
29/30
ProStriata

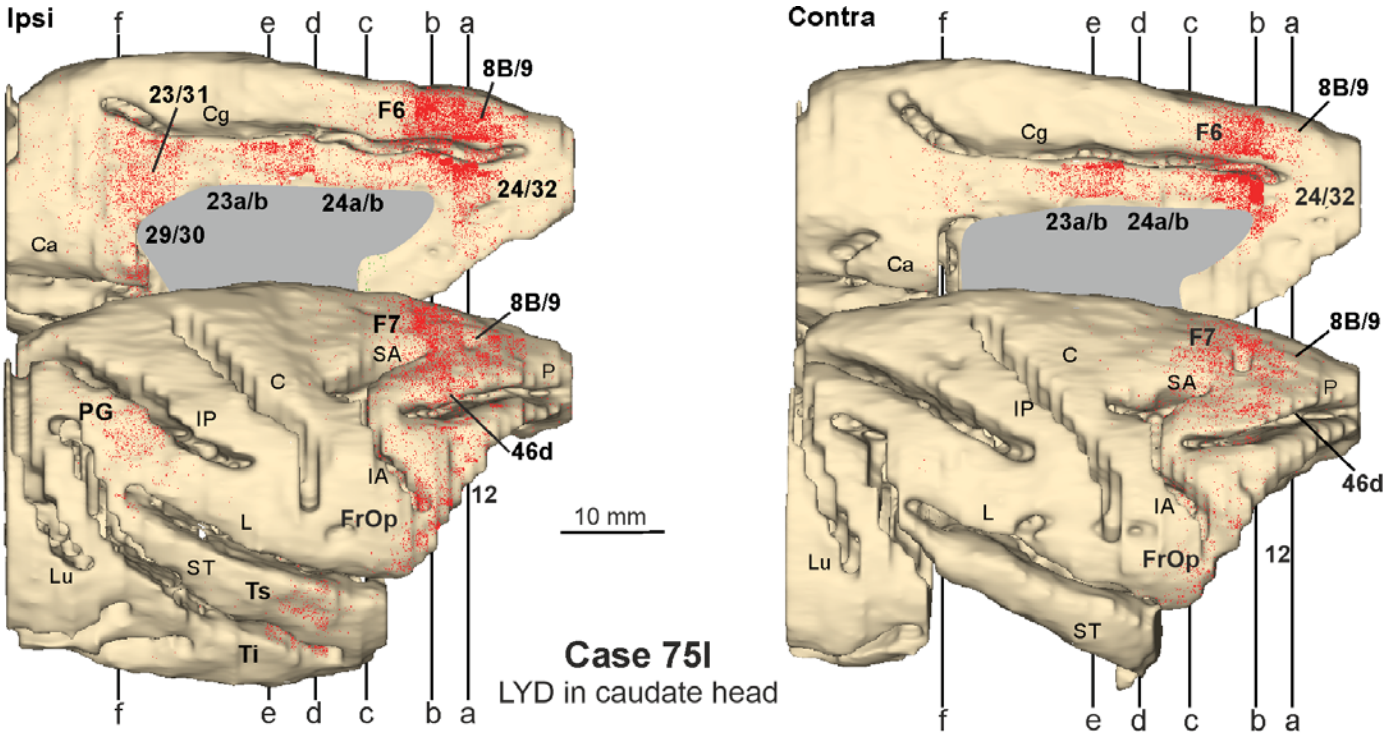
Ipsi
Contra
f e d c b a
8B/9
23/31
Cg
F6
24/32
23a/b
24a/b
29/30
Ca
F7
SA
C
P
PG
IP
46d
IA
12
L
FrOp
Lu
ST
Ts
Ti
10 mm
Case 75l
LYD in caudate head

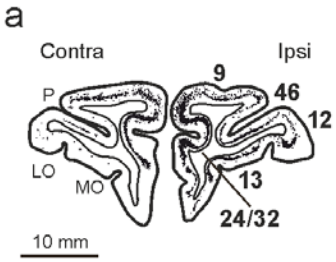
a
Contra
Ipsi
P
9
46
12
LO
MO
13
24/32
10 mm

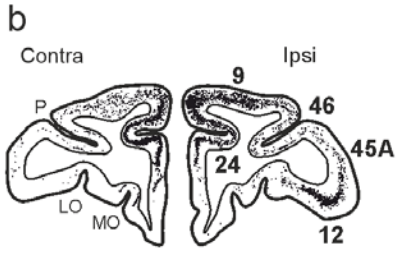
b
Contra
Ipsi
P
9
46
45A
24
LO
MO
12

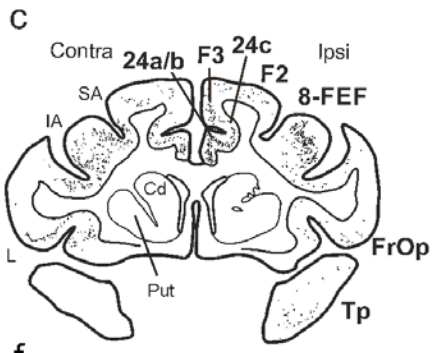
c
Contra
24a/b
F3
24c
F2
Ipsi
SA
8-FEF
IA
Cd
L
FrOp
Put
Tp

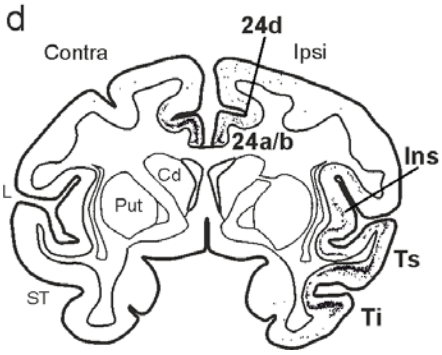
d
24d
Contra
Ipsi
24a/b
Ins
L
Cd
Put
Ts
ST
Ti

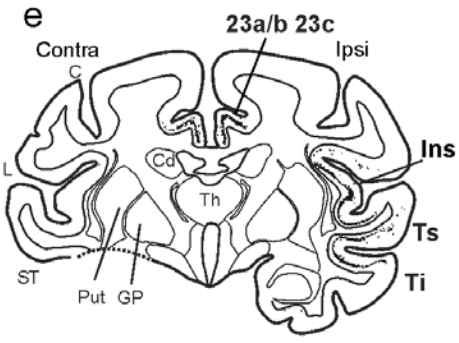
e
23a/b 23c
Contra
Ipsi
C
Ins
L
Cd
Th
Ts
ST
Put
GP
Ti

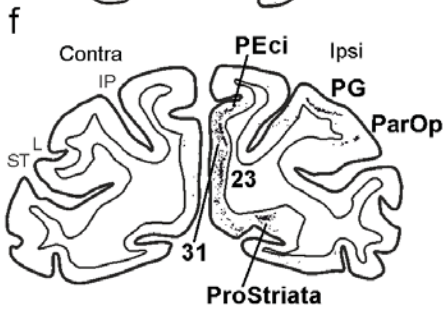
f
Contra
PEci
Ipsi
IP
PG
ParOp
L
ST
23
31
ProStriata

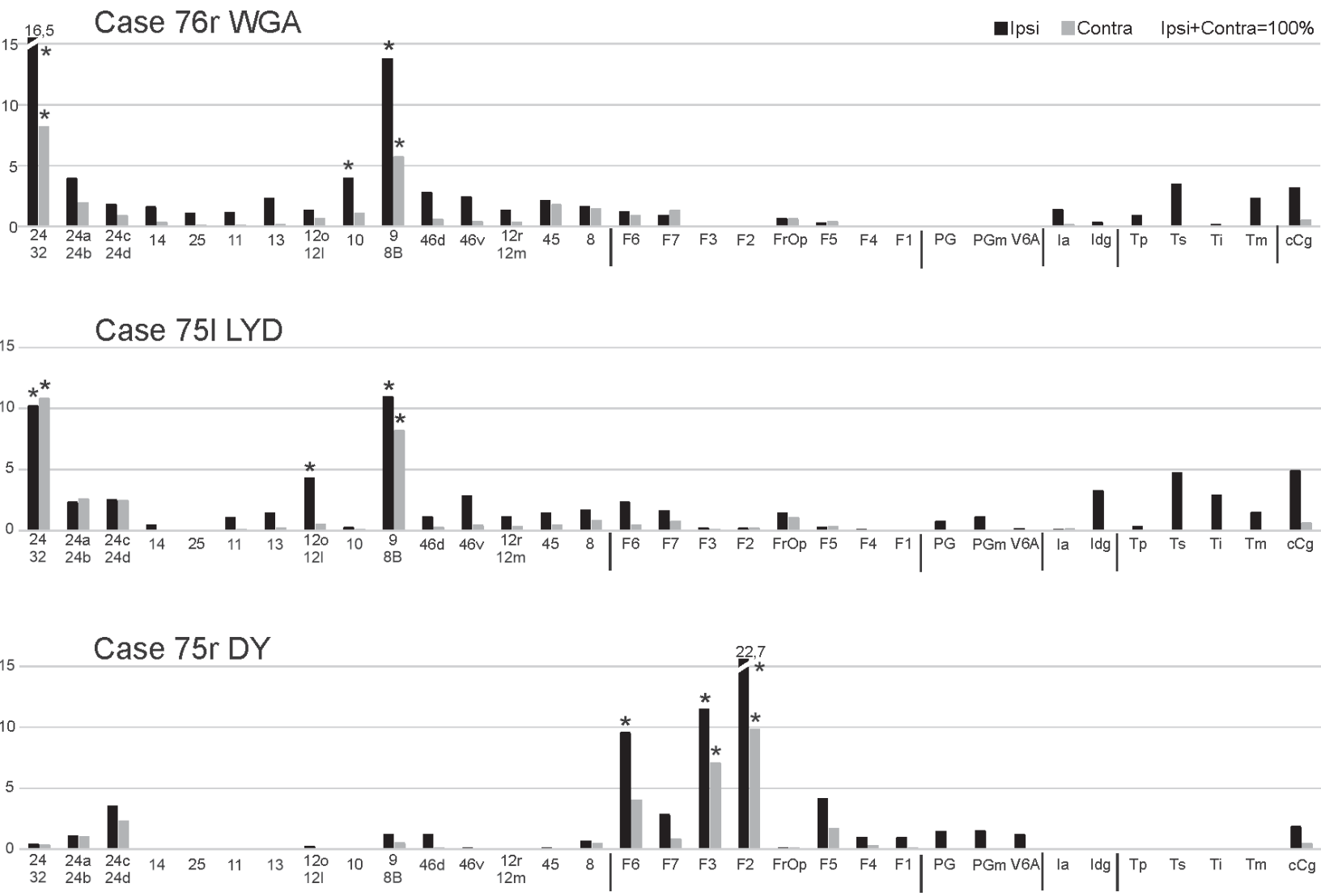
Case 76r WGA
Ipsi
Contra
Ipsi+Contra=100%
16,5
15
10
5
0
24 32
24a 24b
24c 24d
14
25
11
13
12o 12l
10
9 8B
46d
46v
12r 12m
45
8
F6
F7
F3
F2
FrOp
F5
F4
F1
PG
PGm
V6A
Ia
Idg
Tp
Ts
Ti
Tm
cCg

Case 75l LYD
15
10
5
0
24 32
24a 24b
24c 24d
14
25
11
13
12o 12l
10
9 8B
46d
46v
12r 12m
45
8
F6
F7
F3
F2
FrOp
F5
F4
F1
PG
PGm
V6A
Ia
Idg
Tp
Ts
Ti
Tm
cCg

Case 75r DY
22,7
15
10
5
0
24 32
24a 24b
24c 24d
14
25
11
13
12o 12l
10
9 8B
46d
46v
12r 12m
45
8
F6
F7
F3
F2
FrOp
F5
F4
F1
PG
PGm
V6A
Ia
Idg
Tp
Ts
Ti
Tm
cCg

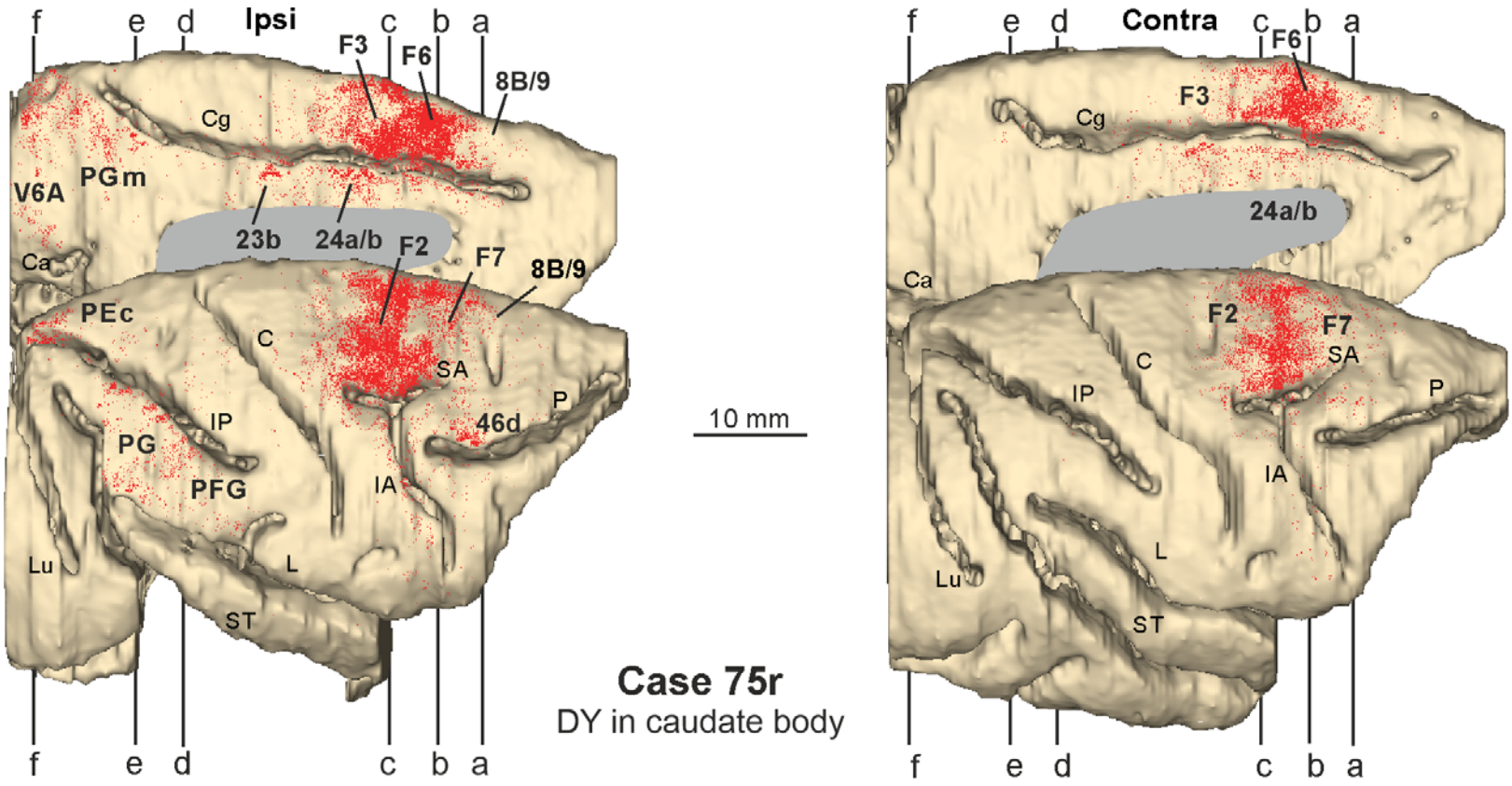
f e d Ipsi c b a
F3
F6
8B/9
Cg
V6A
PGm
23b
24a/b
F2
F7
8B/9
Ca
PEc
C
SA
P
IP
46d
PG
PFG
IA
Lu
L
ST
10 mm
Case 75r
DY in caudate body
f e d Contra c b a
F6
F3
Cg
24a/b
Ca
F2
F7
SA
C
IP
P
IA
L
Lu
ST

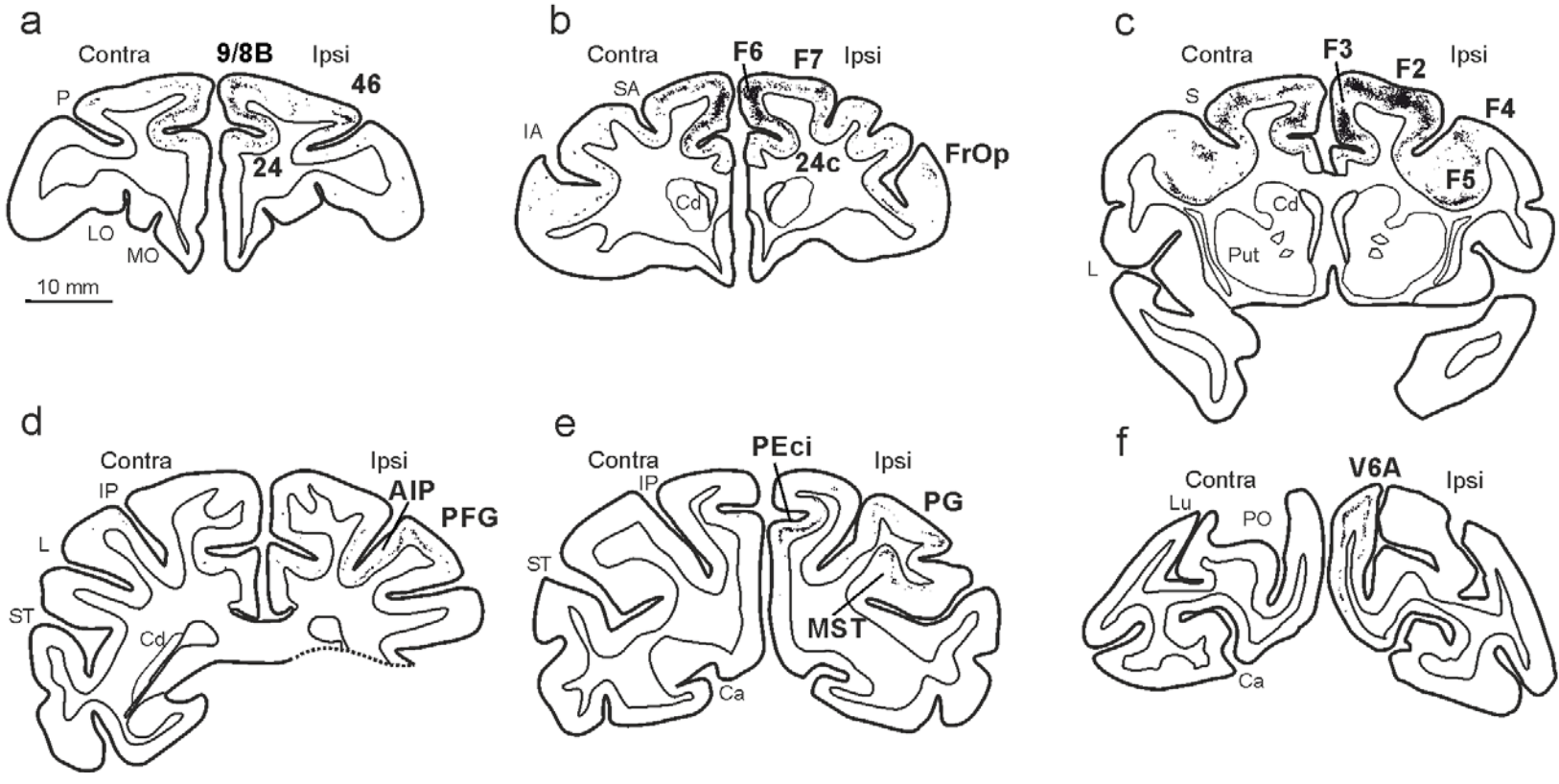
a
Contra
9/8B
Ipsi
46
P
24
LO
MO
10 mm
b
Contra
F6
F7
Ipsi
SA
IA
24c
FrOp
Cd
c
Contra
F3
F2
Ipsi
S
F4
F5
Cd
Put
L
d
Contra
Ipsi
IP
AIP
PFG
L
ST
Cd
e
Contra
PEci
Ipsi
IP
PG
ST
MST
Ca
f
Contra
V6A
Ipsi
Lu
PO
Ca

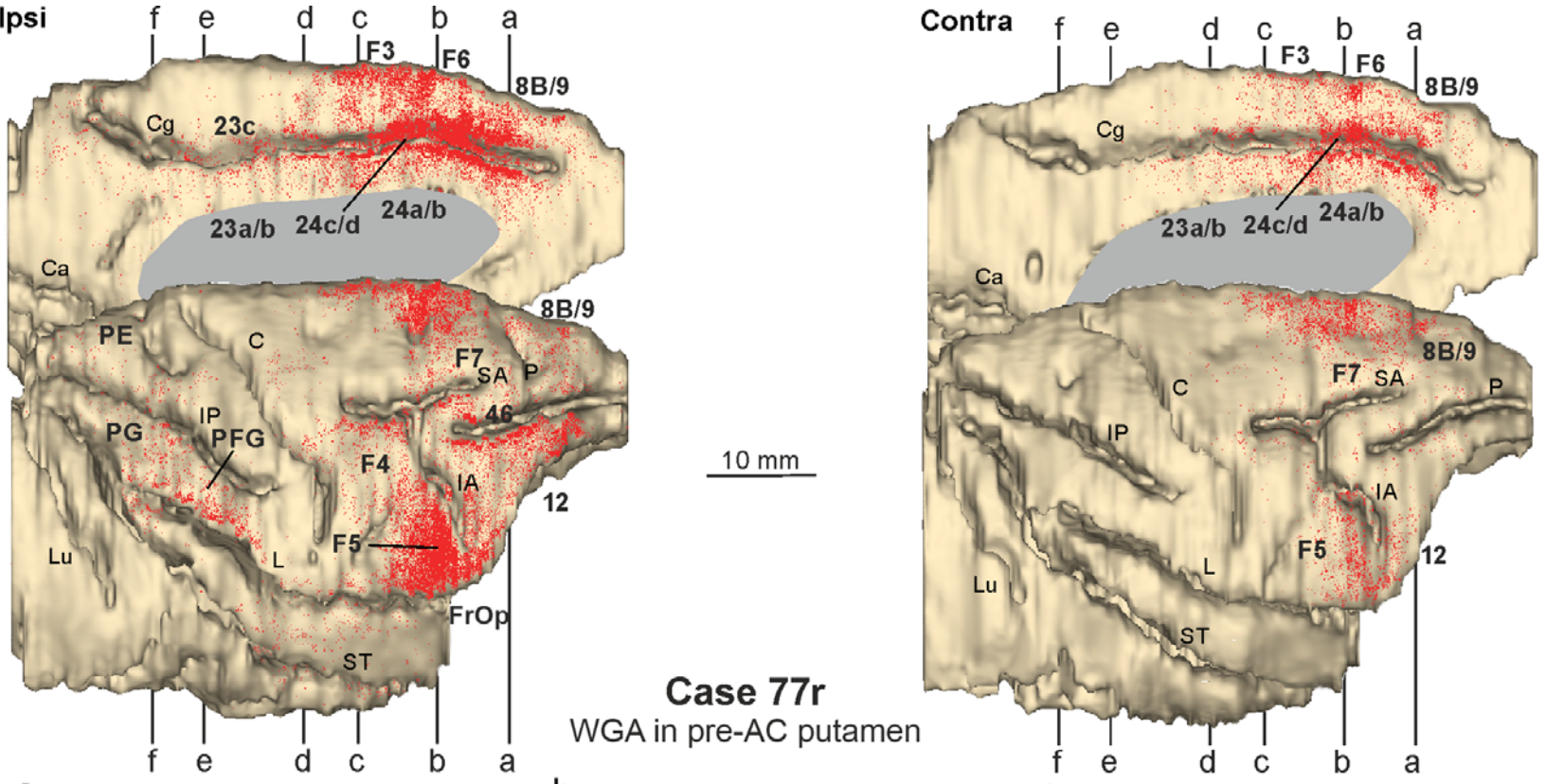

Case 77r

WGA in pre-AC putamen

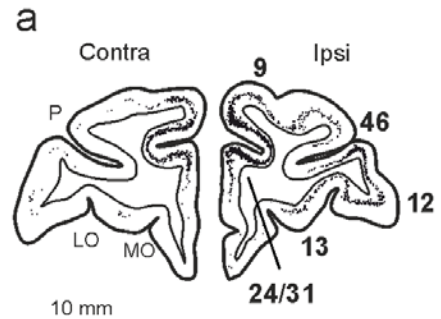

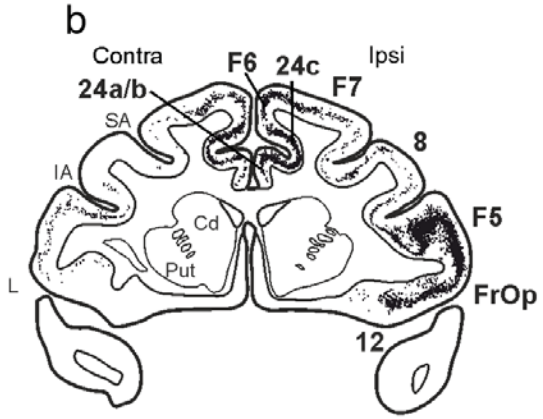

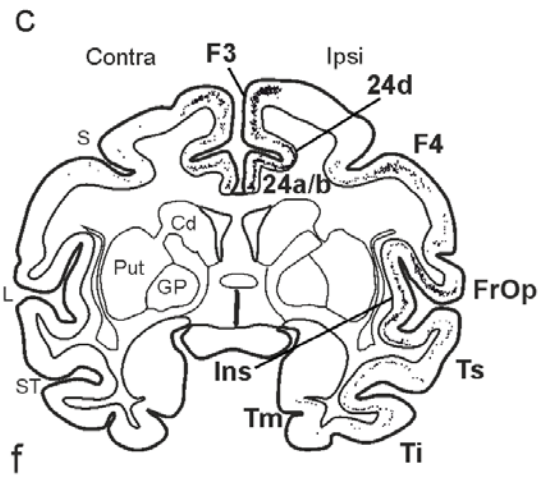

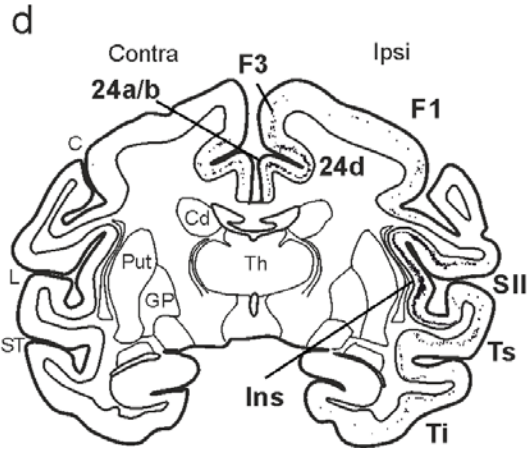

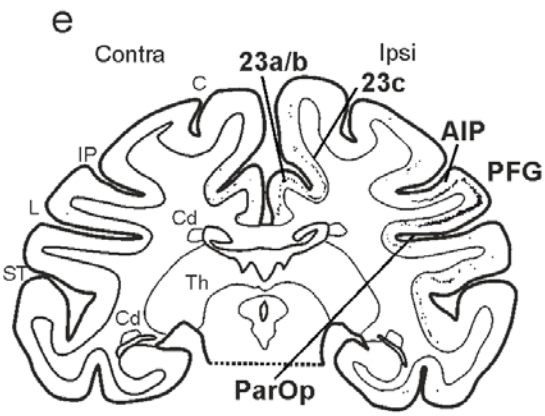

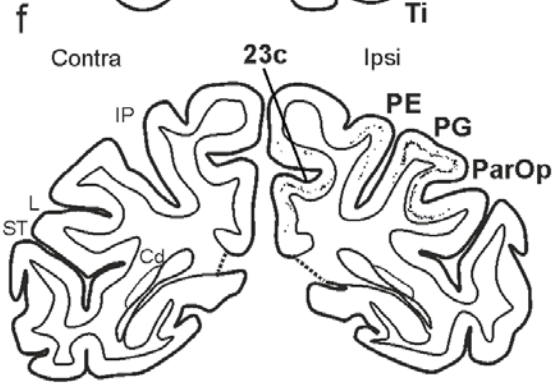

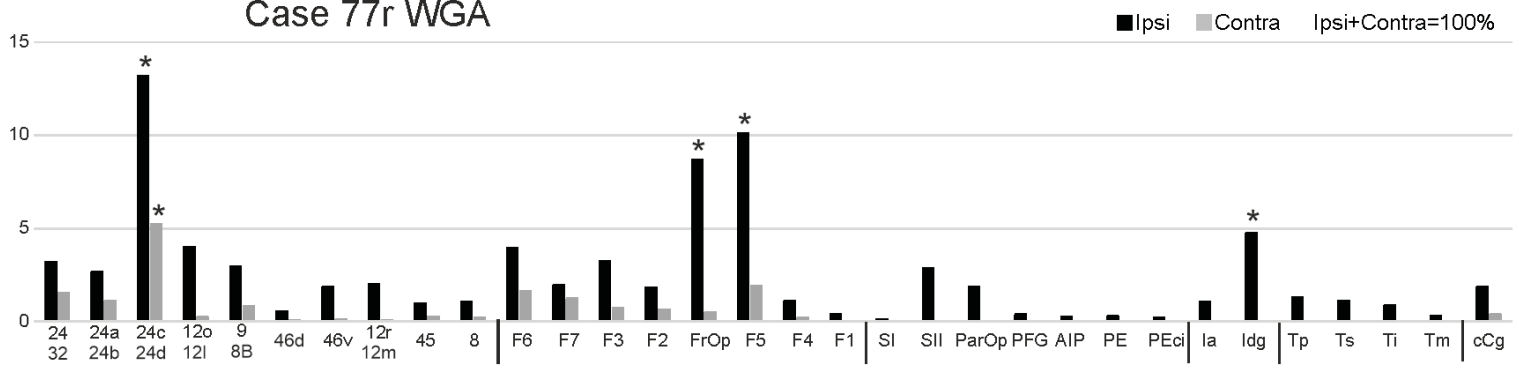
Case 77r WGA
Ipsi
Contra
Ipsi+Contra=100%
15
10
5
0
24 32
24a 24b
24c 24d
12o 12l
9 8B
46d
46v
12r 12m
45
8
F6
F7
F3
F2
FrOp
F5
F4
F1
SI
SII
ParOp
PFG
AIP
PE
PEci
Ia
Idg
Tp
Ts
Ti
Tm
cCg

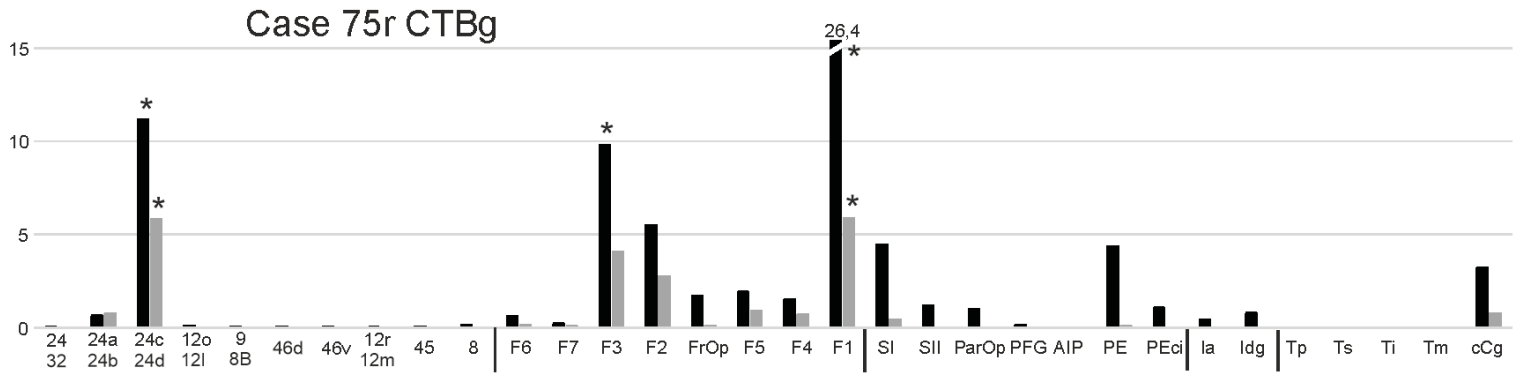
Case 75r CTBg
26,4
15
10
5
0
24 32
24a 24b
24c 24d
12o 12l
9 8B
46d
46v
12r 12m
45
8
F6
F7
F3
F2
FrOp
F5
F4
F1
SI
SII
ParOp
PFG
AIP
PE
PEci
Ia
Idg
Tp
Ts
Ti
Tm
cCg

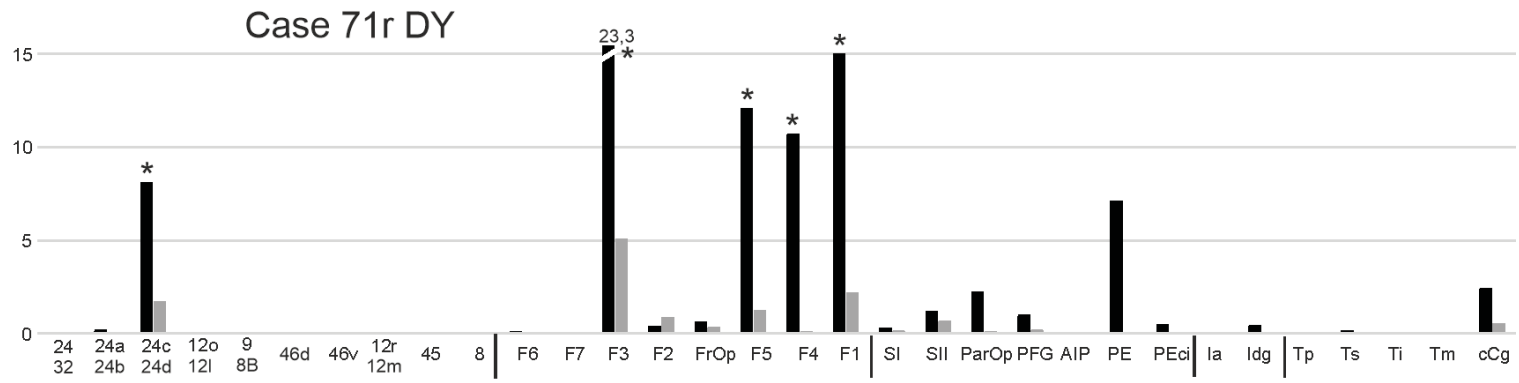
Case 71r DY
23,3
15
10
5
0
24 32
24a 24b
24c 24d
12o 12l
9 8B
46d
46v
12r 12m
45
8
F6
F7
F3
F2
FrOp
F5
F4
F1
SI
SII
ParOp
PFG
AIP
PE
PEci
Ia
Idg
Tp
Ts
Ti
Tm
cCg

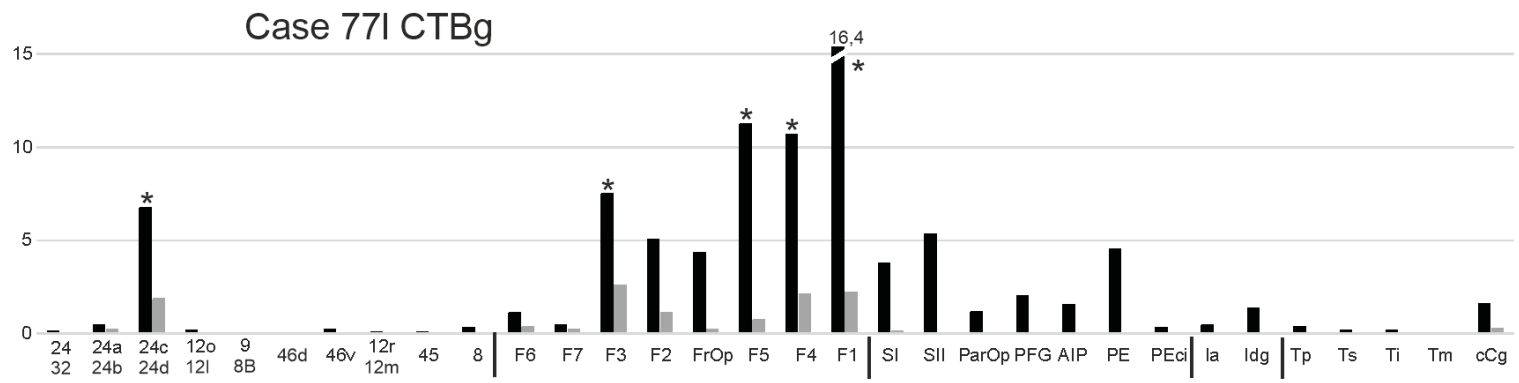
Case 77l CTBg
16,4
15
10
5
0
24 32
24a 24b
24c 24d
12o 12l
9 8B
46d
46v
12r 12m
45
8
F6
F7
F3
F2
FrOp
F5
F4
F1
SI
SII
ParOp
PFG
AIP
PE
PEci
Ia
Idg
Tp
Ts
Ti
Tm
cCg

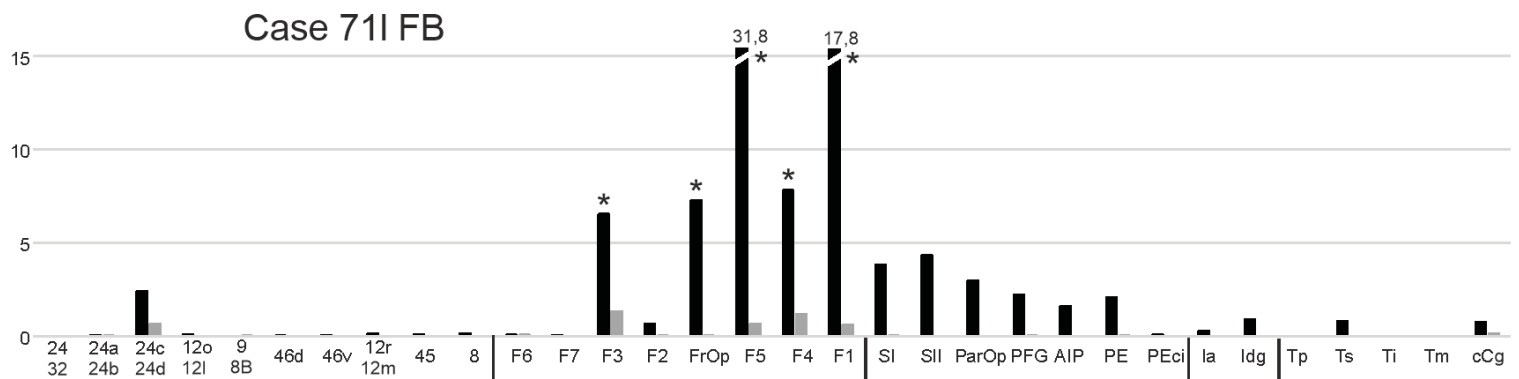
Case 71l FB
31,8
17,8
15
10
5
0
24 32
24a 24b
24c 24d
12o 12l
9 8B
46d
46v
12r 12m
45
8
F6
F7
F3
F2
FrOp
F5
F4
F1
SI
SII
ParOp
PFG
AIP
PE
PEci
Ia
Idg
Tp
Ts
Ti
Tm
cCg

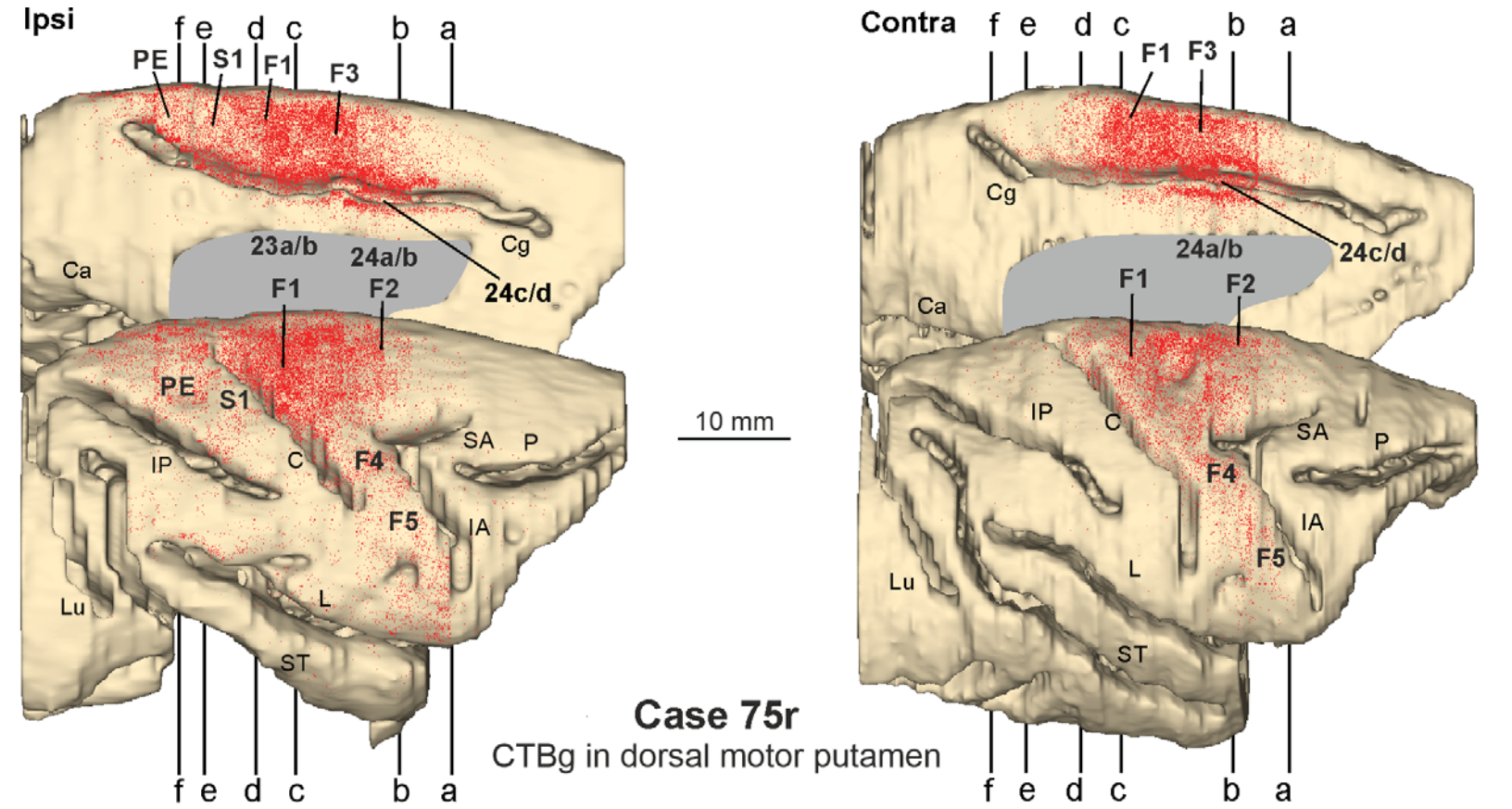

Case 75r

CTBg in dorsal motor putamen

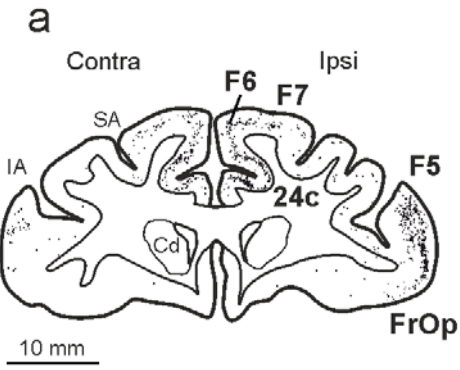

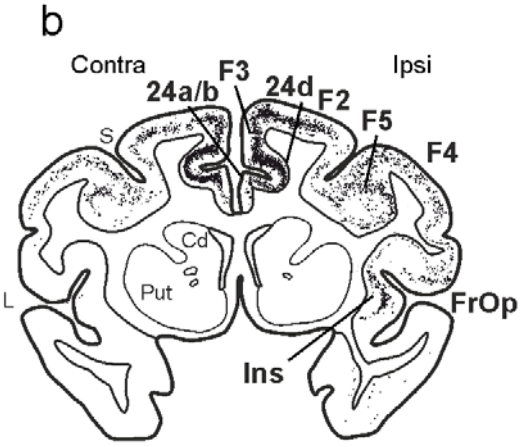

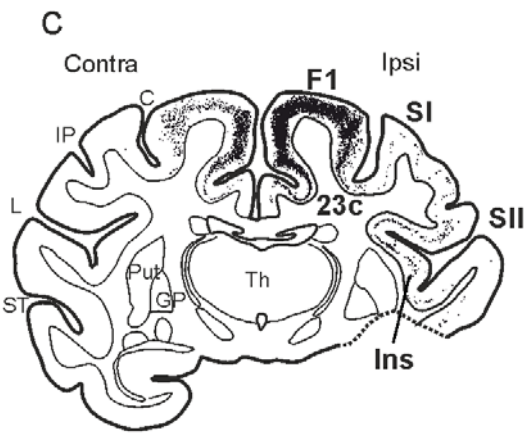

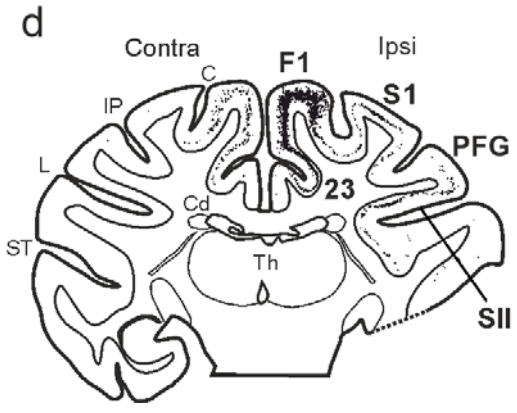

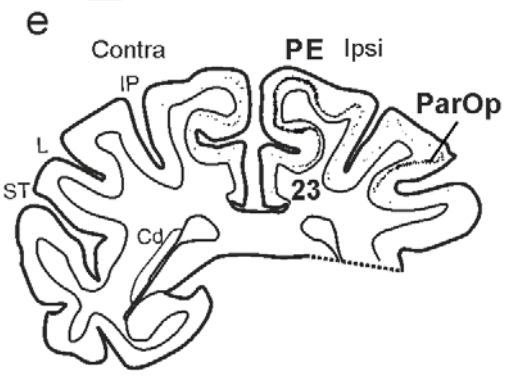

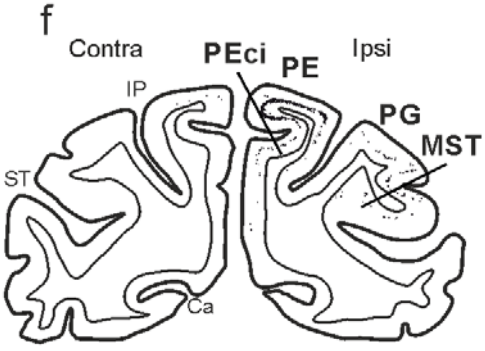

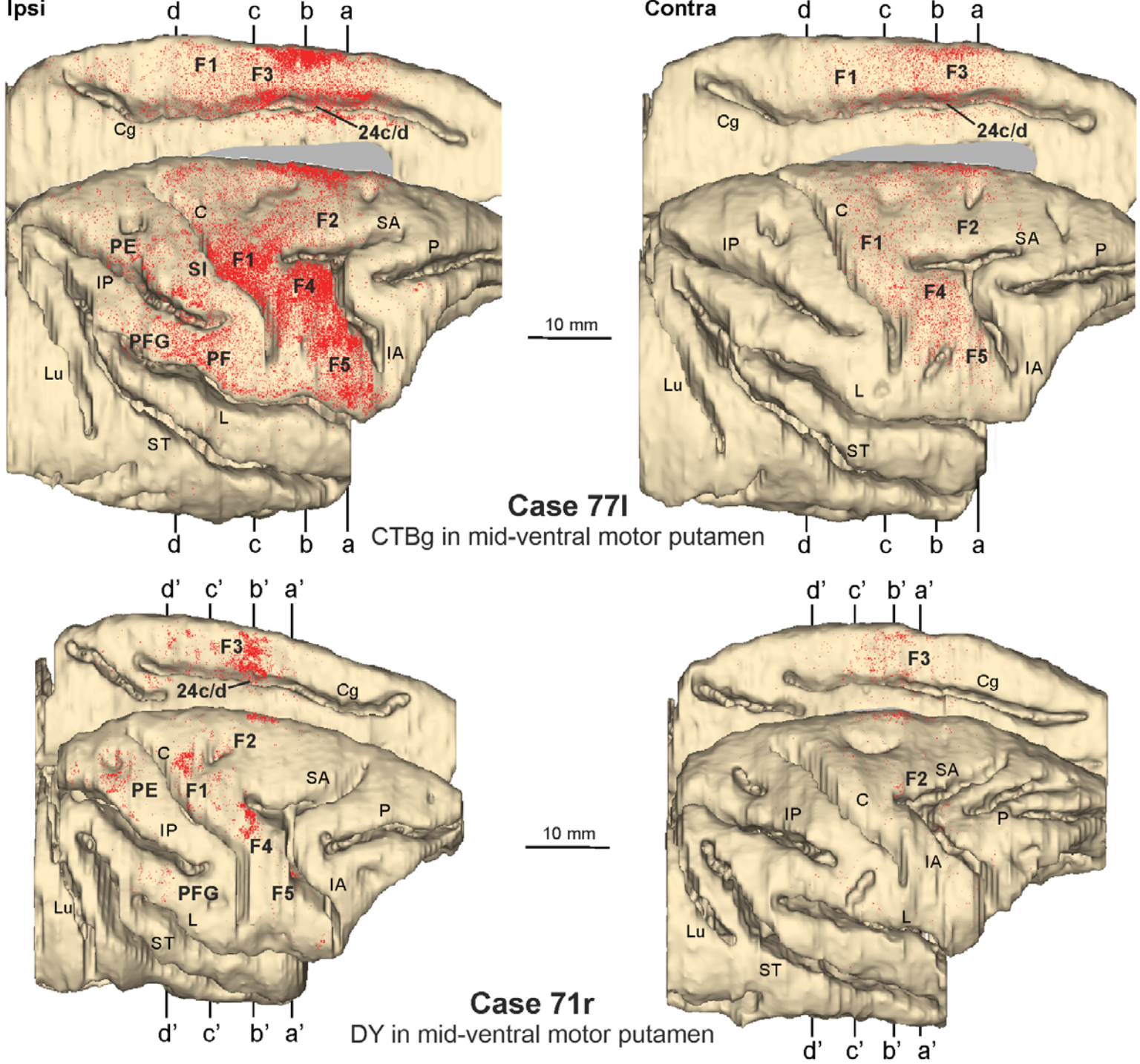
Ipsi
Contra
d c b a
F1
F3
Cg
24c/d
C
F2
SA
P
PE
SI
IP
F4
PFG
PF
F5
IA
Lu
L
ST
10 mm
Case 77l
CTBg in mid-ventral motor putamen
d' c' b' a'
24c/d
Case 71r
DY in mid-ventral motor putamen
d'' c'' b''a''
FrOp
Case 71l
FB in mid-ventral motor putamen

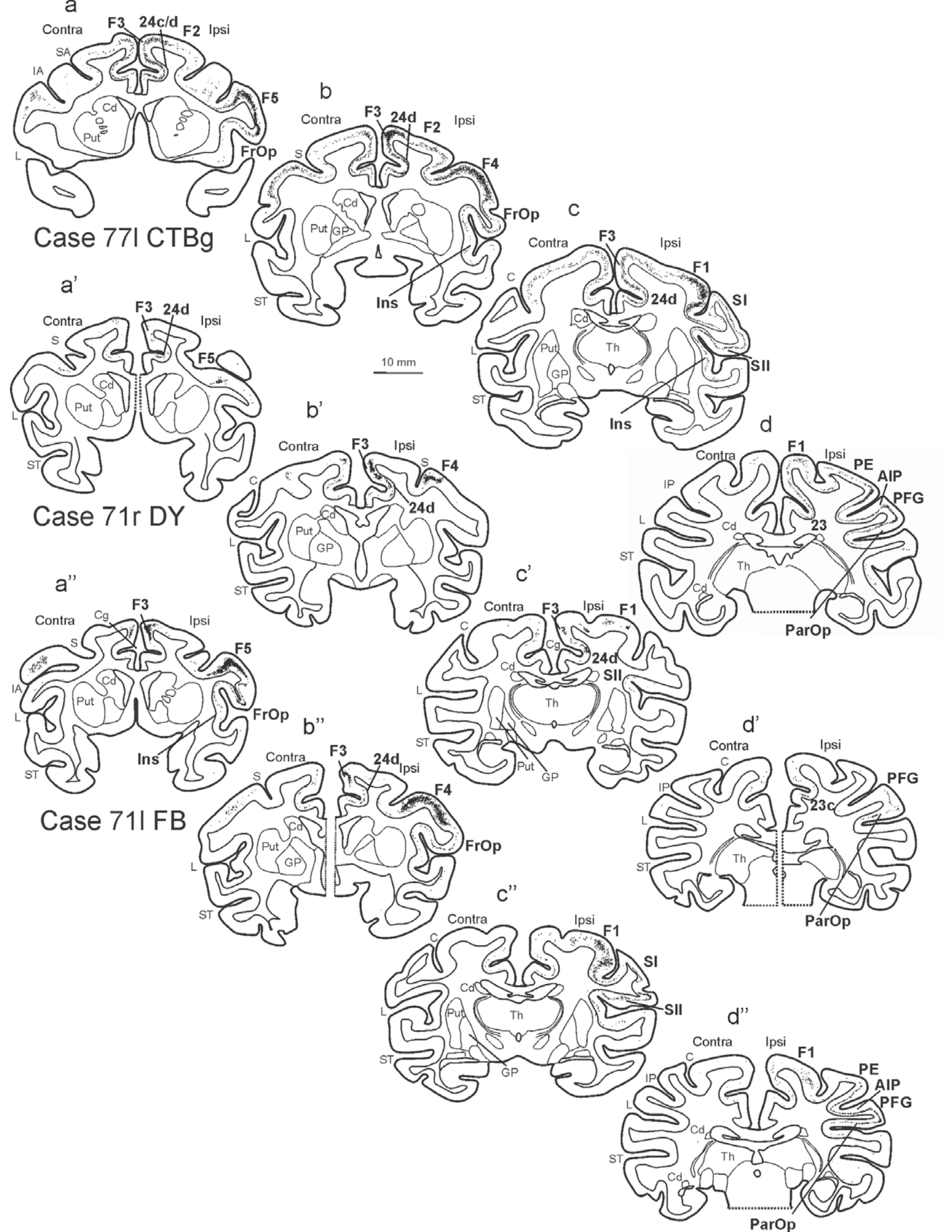
a
Contra
F3
24c/d
F2
Ipsi
SA
IA
F5
Cd
Put
L
FrOp
b
Contra
F3
24d
F2
Ipsi
S
F4
Cd
Put
GP
L
FrOp
Ins
ST
Case 77l CTBg
c
Contra
F3
Ipsi
F1
C
24d
SI
Cd
Put
Th
L
SII
GP
ST
Ins
a'
Contra
F3
24d
Ipsi
S
F5
Cd
Put
L
ST
10 mm
b'
Contra
F3
Ipsi
S
F4
C
24d
Cd
Put
GP
L
ST
Case 71r DY
d
Contra
F1
Ipsi
PE
AIP
PFG
IP
L
Cd
23
ST
Th
Cd
ParOp
a''
Contra
Cg
F3
Ipsi
S
F5
IA
Cd
Put
L
FrOp
ST
Ins
c'
Contra
F3
Ipsi
F1
C
Cg
Cd
24d
SII
L
Th
ST
Put
GP
b''
Contra
F3
24d
Ipsi
S
F4
Cd
Put
GP
L
FrOp
ST
Case 71l FB
d'
Contra
Ipsi
C
PFG
IP
23c
L
Th
ST
ParOp
c''
Contra
Ipsi
F1
C
SI
Cd
Th
L
Put
SII
ST
GP
d''
Contra
Ipsi
F1
C
PE
AIP
IP
PFG
L
Cd
Th
ST
Cd
ParOp

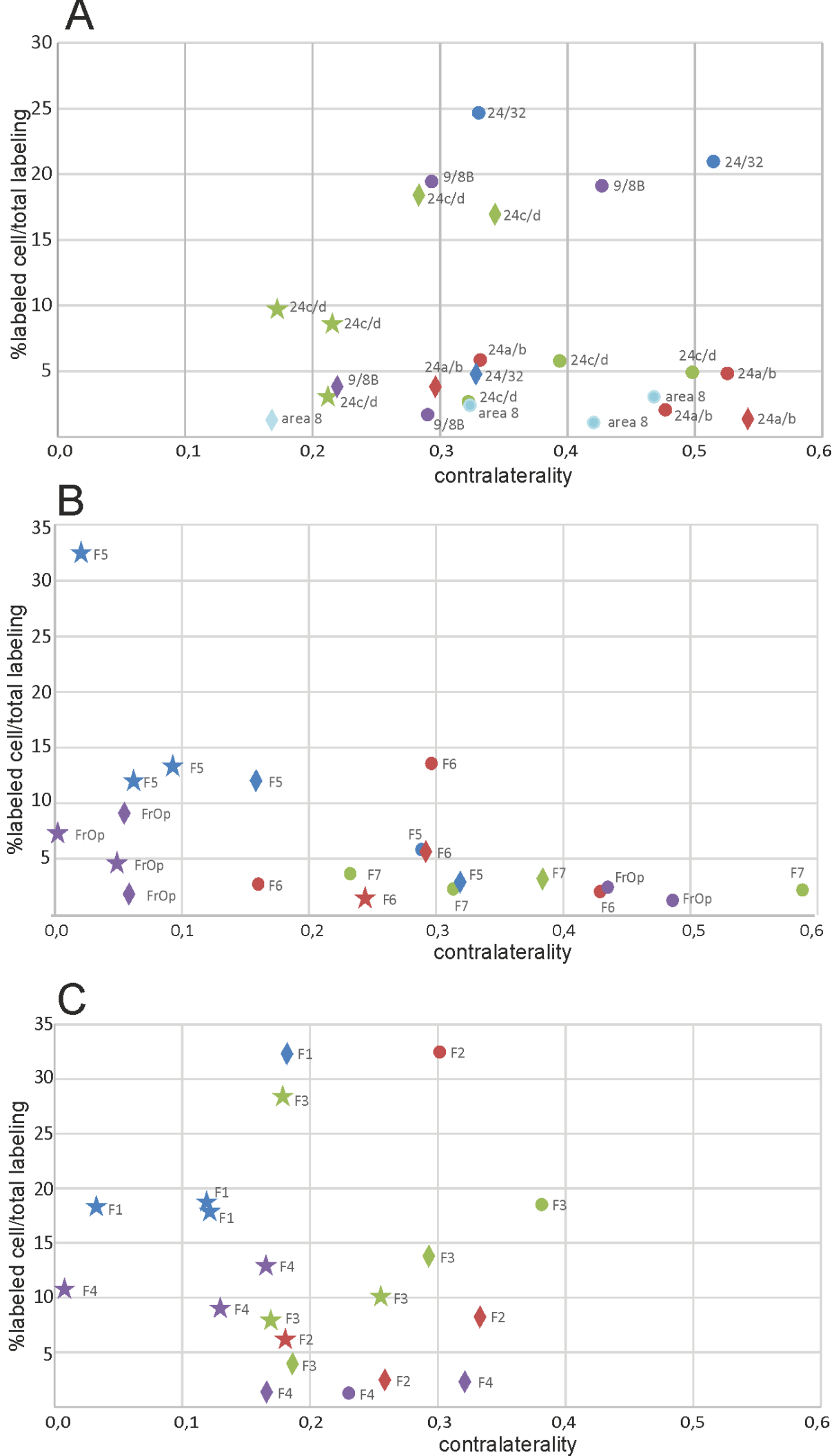
A
%labeled cell/total labeling
contralaterality
24/32
9/8B
24c/d
24a/b
area 8
B
%labeled cell/total labeling
contralaterality
F5
F6
F7
FrOp
C
%labeled cell/total labeling
contralaterality
F1
F2
F3
F4